RESEARCH ARTICLE

JBMR®

# Osteocyte RANKL Drives Bone Resorption in Mouse Ligature-Induced Periodontitis

Mizuho Kittaka,[1,2] Tetsuya Yoshimoto,[1,2] Marcus E Levitan,[1,2] Rina Urata,[1,2] Roy B Choi,[2,3] Yayoi Teno,[1,2] Yixia Xie,[4] Yukiko Kitase,[2,3] Matthew Prideaux,[2,3] Sarah L Dallas,[4] Alexander G Robling,[2,3] and Yasuyoshi Ueki[1,2]

[1]Department of Biomedical Sciences and Comprehensive Care, Indiana University School of Dentistry, Indianapolis, IN, USA
[2]Indiana Center for Musculoskeletal Health, Indiana University School of Medicine, Indianapolis, IN, USA
[3]Department of Anatomy, Cell Biology, and Physiology, Indiana University School of Medicine, Indianapolis, IN, USA
[4]Department of Oral and Craniofacial Sciences, University of Missouri Kansas City, School of Dentistry, Kansas City, MO, USA

## ABSTRACT

Mouse ligature-induced periodontitis (LIP) has been used to study bone loss in periodontitis. However, the role of osteocytes in LIP remains unclear. Furthermore, there is no consensus on the choice of alveolar bone parameters and time points to evaluate LIP. Here, we investigated the dynamics of changes in osteoclastogenesis and bone volume (BV) loss in LIP over 14 days. Time-course analysis revealed that osteoclast induction peaked on days 3 and 5, followed by the peak of BV loss on day 7. Notably, BV was restored by day 14. The bone formation phase after the bone resorption phase was suggested to be responsible for the recovery of bone loss. Electron microscopy identified bacteria in the osteocyte lacunar space beyond the periodontal ligament (PDL) tissue. We investigated how osteocytes affect bone resorption of LIP and found that mice lacking receptor activator of NF-κB ligand (RANKL), predominantly in osteocytes, protected against bone loss in LIP, whereas recombination activating 1 (RAG1)-deficient mice failed to resist it. These results indicate that T/B cells are dispensable for osteoclast induction in LIP and that RANKL from osteocytes and mature osteoblasts regulates bone resorption by LIP. Remarkably, mice lacking the myeloid differentiation primary response gene 88 (MYD88) did not show protection against LIP-induced bone loss. Instead, osteocytic cells expressed nucleotide-binding oligomerization domain containing 1 (NOD1), and primary osteocytes induced significantly higher *Rankl* than primary osteoblasts when stimulated with a NOD1 agonist. Taken together, LIP induced both bone resorption and bone formation in a stage-dependent manner, suggesting that the selection of time points is critical for quantifying bone loss in mouse LIP. Pathogenetically, the current study suggests that bacterial activation of osteocytes via NOD1 is involved in the mechanism of osteoclastogenesis in LIP. The NOD1-RANKL axis in osteocytes may be a therapeutic target for bone resorption in periodontitis. © 2023 The Authors. *Journal of Bone and Mineral Research* published by Wiley Periodicals LLC on behalf of American Society for Bone and Mineral Research (ASBMR).

**KEY WORDS:** LIGATURE-INDUCED PERIODONTITIS; OSTEOCYTES; OSTEOCLASTS; NOD1; RANKL

## Introduction

Periodontitis is a bacteria-driven inflammatory disease of the oral cavity that ultimately leads to tooth loss due to excessive alveolar bone resorption. It is highly prevalent and a leading cause of tooth loss worldwide.[1,2] However, although increased osteoclastogenesis is known to play a critical role in alveolar bone destruction in periodontitis, the underlying mechanism that promotes osteoclastogenesis in the disease is not fully understood. To study the molecular and cellular mechanisms of bone destruction in periodontitis, the ligature-induced periodontitis (LIP) model has been widely used.[3-5] In this model, increased bacterial load due to the accumulation of oral commensal bacteria in and around silk sutures is a primary cause of periodontitis leading to alveolar bone loss.[6,7] LIP was first established in rats and dogs.[6,8] Currently, the application of LIP has been successfully extended to mice as a result of overcoming technical difficulties and the advantage of the availability of a


Received in original form February 25, 2023; revised form July 29, 2023; accepted August 4, 2023.
Address correspondence to: Yasuyoshi Ueki, MD, PhD, Department of Biomedical Sciences and Comprehensive Care, Indiana University School of Dentistry, Indiana Center for Musculoskeletal Health, Indiana University School of Medicine, Van Nuys Medical Science Building, Room 514, 635 Barnhill Drive, Indianapolis, IN 46202-5126, USA. E-mail: uekiy@iu.edu
Additional Supporting Information may be found in the online version of this article.
Journal of Bone and Mineral Research, Vol. 38, No. 10, October 2023, pp 1521–1540.

DOI: 10.1002/jbmr.4897

wide range of genetically engineered strains and disease models.[5,7,9,10]

Although LIP has become a valuable model for studying human periodontitis and periodontitis-induced alveolar bone resorption,[5] the underlying mechanisms of how oral commensal bacteria drive LIP and how LIP leads to alveolar bone loss are not fully defined. In addition, there is no clear consensus on the optimal time points for phenotypic analysis of LIP mice. Consequently, different time points between 5 and 28 days after LIP induction have been chosen to study alveolar bone loss and gingival inflammation.[11-13] Recently, a time-course study was performed in a simplified suture-insertion periodontitis model. This study showed that the distance between the cementoenamel junction (CEJ) and the alveolar bone crest (ABC), a parameter of alveolar bone loss, began to increase after day 6, but it plateaued after day 9 through day 18.[14] Furthermore, this study found that the inflammatory profiles of gingival tissues are significantly variable during the disease process, suggesting that the pathophysiology of LIP may be more dynamic and that the time points chosen for analysis are critical for the accurate assessment of alveolar bone loss and periodontal inflammation in the LIP model. Accordingly, more detailed time-course studies of alveolar bone loss and gingival inflammation in relation to oral tissue bacterial load will be essential to better understand the pathogenesis of LIP and human periodontitis.

In addition to the poor understanding of stage-specific LIP pathology, the parameters used to assess alveolar bone mass have been controversial in LIP studies. In the long bone and vertebra, three-dimensional (3D) volumetric analysis by microcomputed tomography (μCT) provides standard parameters, including bone volume/tissue volume (BV/TV), for quantifying bone mass. Similarly, previous studies using *Porphyromonas gingivalis* (*Pg*)- or its lipopolysaccharide-induced mouse periodontitis models have shown that 3D BV analysis with μCT is advantageous for sensitive detection and accurate quantification of alveolar bone mass.[15,16] Nevertheless, one-dimensional (1D) linear analysis of the CEJ-ABC distance has still been predominantly used to quantify and compare alveolar bone loss in the LIP model, presumably because of the traditional assumption that the ABC is the primary site of the bone resorption in LIP.[7,11,12,14,17] As a result, the use of 3D BV analysis in the LIP model has been limited and uncommon.

The receptor-activator of nuclear factor-κB ligand (RANKL, encoded by the *Tnfsf11* gene) is the master cytokine responsible for osteoclast differentiation and drives bone resorption in LIP.[12,18,19] In particular, osteocyte RANKL has been shown to play a critical role in bone resorption under physiological and pathological conditions.[20-28] However, the impact of osteocyte RANKL on bone resorption in LIP remains unknown. Furthermore, although a variety of bacterial pathogen-associated molecular patterns (PAMPs) have been shown to induce RANKL expression in osteocytic cells,[28,29] the impact of nucleotide-binding oligomerization domain containing 1 (NOD1)-mediated signaling pathways, which is known to regulate LIP-induced alveolar bone osteolysis,[30] on osteocyte RANKL expression remains uninvestigated.

The main aim of this study was to investigate the mechanism by which excessive commensal bacterial load leads to periodontitis and alveolar bone destruction using the LIP model. We hypothesized that the impact of ligature placement is dynamic and time-dependent and that osteocyte RANKL is important for bone loss in LIP. Here, we show that LIP not only causes osteoclastic bone loss but also leads to tooth displacement and bone formation. Time-course characterization of LIP in mice showed that osteoclast induction was transient and peaked on days 3 to 5. BV loss was detected by day 5. A significant increase in the CEJ-ABC distance was observed after day 7. Tooth displacement from day 1 affected the measurement of the CEJ-ABC distance even before the osteoclast induction phase. Notably, BV was recovered by day 14. LIP caused bacterial invasion even into the osteocyte lacunar-canalicular system beyond the gingival and periodontal ligament tissues. Genetically, none of the mice lacking recombination activating 1 (RAG1), toll-like receptor (TLR) 2/4, or myeloid differentiation primary response 88 (MYD88) protected against bone loss in LIP. Instead, the deletion of RANKL in osteocytes and mature osteoblasts blocked it. In vitro, osteocytic cells expressed NOD1 protein, and activation of the NOD1 pathway induced *Rankl* expression in primary osteocytes more robustly than in primary osteoblasts. Therefore, the current study provides insights into the dynamics of LIP pathology and suggests an essential role of bacterially stimulated osteocytes as RANKL suppliers in mouse LIP and potentially in human periodontitis.

## Materials and Methods

### Mice

All animal experiments were performed under the animal protocol approved by the IACUC of Indiana University School of Medicine. All mice were bred and housed under specific-pathogen-free (SPF) conditions. Animals were group-housed on a 12-hour light/dark cycle with *ad libitum* food (2018SX Envigo [-Indianapolis, IN, USA], 18% protein extruded rodent diet) and water. $Rankl^{fl/fl}$ (018978), *Dmp1-Cre* (023047), *Col1a1-*$Cre^{ERT2}$ (016241), $Rag1^{-/-}$ (002216), *Ai9* (007909), $Tlr2^{-/-}$ (004650), $Tlr4^{lps\text{-}del/lps\text{-}del}$ (007227), $Myd88^{-/-}$ (009088), and wild-type mice on the C57BL/6 background were obtained from the Jackson Laboratory (Bar Harbor, ME, USA). $Rankl^{fl/fl}$ mice carrying *Col1a1-*-$Cre^{ERT2}$ and their littermate $Rankl^{fl/fl}$ control mice received tamoxifen (2 mg/mouse/d) intraperitoneally for 5 consecutive days to induce *Cre*-mediated gene recombination.[31] We found that *Dmp1-Cre* deleted the target gene in the germline at a low frequency (less than 5%, but it depends on the target gene; MK, TY, and YU, personal communication). To identify *Rankl*-deleted mice in the germline, we performed PCR genotyping with tail DNA using three primers that detect all wild-type, floxed (*fl*), and deleted alleles. Mice carrying the *Rankl* deletion in the germline were excluded from the study. Primer sequences for genotyping are listed in Supplemental Table S1.

### Ligature-induced periodontitis (LIP)

The maxillary left second molar of 10-week-old female and male mice was ligated with 5-0 silk suture (Ethicon, Somerville, NJ, USA) for up to 14 days. The right second molar was left unligated to serve as a control of alveolar bone analysis. To deplete oral microbes, mice were treated with a broad-spectrum antibiotics cocktail (1.0 g/L ampicillin, 0.5 g/L vancomycin, and 1.0 g/L kanamycin, Gold Biotechnology, Olivette, MO, USA) in drinking water and daily administration of 1.6 mg metronidazole (Alfa Aesar, Haverhill, MA, USA) by oral gavage starting from 5 days before LIP induction until analysis. For LIP with zoledronate acid treatment, mice were administered 200 μg/kg zoledronic acid (Zometa, Novartis, Stein, Switzerland; diluted with saline) intraperitoneally twice a week starting from 1 week before LIP

induction until analysis. Males and females were analyzed separately. For *Col1a1-Cre*$^{ERT2}$;*Rankl*$^{fl/fl}$ mice, LIP was induced 2 days after the final tamoxifen injection.

### μCT analysis

Maxillae were fixed with 4% paraformaldehyde (PFA) in PBS for 24 hours and soaked in 70% ethanol before scanning with the Skyscan 1176 (Bruker, Kontich, Belgium). The following conditions were used: 50 kV, 8.43-μm pixel size, 0.3-degree rotation step, and 926-ms exposure time. Scanned data were reconstructed with NRecon software (Bruker) with the dynamic range from 0 to 0.12. The 3D images were aligned with the DataViewer (Bruker). For volumetric analysis, alveolar bone between two buccal roots underneath the maxillary second molar, which is composed of 16 slices (approximately 135-μm thickness), was segmented as a region of interest (ROI).[9,10] Bone volume (BV) was measured by the CT-Analyzer (Bruker) with a threshold value of 60. The following formula, {(BV of unligated side − BV of ligated side)/BV of unligated side} × 100, was used to calculate the percentage of bone loss. Mice having fused two roots were excluded from BV analysis. The total distance between cementoenamel junction and alveolar bone crest (CEJ-ABC) underneath the four cusps of the second molar was measured three times and averaged. The total width of the periodontal ligament (PDL) underneath the second molar was measured in the four 2D μCT images that were used for the CEJ-ABC measurement. All μCT analyses were performed by personnel who were blinded to genotype or treatment information.

### Histology and histomorphometry

After μCT analysis, jawbone tissues were decalcified with EDTA (0.5 M, pH = 7.2), then embedded with paraffin. Tissues were sectioned in the coronal plane at a thickness of 6 μm and subjected to H&E, tartrate-resistant acid phosphatase (TRAP), and immunohistochemical staining. For histomorphometric analysis of osteoclasts, the number of osteoclasts (N.Oc), osteoclast surface (Oc.S), bone surface (BS), and bone area (BA) were measured on TRAP-stained sections of alveolar bone between two buccal roots of the maxillary second molar using ImageJ (NIH).[32] Osteoblast surface was measured on toluidine blue–stained sections. Cuboidal cells on the bone surface forming a cluster with more than 3 cells were counted as osteoblasts. Results from two sections separated by 20 to 50 μm were averaged. Bone samples from unligated mice or unligated right side were used as controls. Measurements were performed by personnel blinded to sample information.

### Alkaline phosphatase staining

Paraffin sections were deparaffinized, rehydrated, and then incubated with NTM solution (100 mM Tris pH 9.0, 50 mM $MgCl_2$, 100 mM NaCl, and 0.1% Tween 20) at 37°C for 30 minutes. Then, sections were incubated with alkaline phosphatase (ALP) staining solution (consisting of NTM solution supplemented with 0.5% nitro blue tetrazolium chloride and 0.375% 5-Bromo-4-chloro-3-indolyl phosphate) at 37°C for 16 hours. Nuclear fast red was used for counterstaining.

### Immunohistochemical (IHC) staining

Deparaffinized paraffin sections were rehydrated and incubated with 20 μg/mL of proteinase K (50 mM Tris–HCl, 1 mM EDTA, pH 8.0) for 5 minutes at room temperature, followed by treatment with 3% $H_2O_2$ for 10 minutes. After blocking with 2% rabbit serum/PBS, sections were incubated with anti-neutrophil/monocyte antibody (NIMP-R14, Santa Cruz Biotechnology, Dallas, TX, USA), anti-macrophage antibody (anti-F4/80, AbD17867, Bio-Rad, Hercules, CA, USA) or control rat IgG at 4°C for overnight, followed by incubation with biotinylated rabbit anti-rat IgG (BA-4001, Vector Laboratories, Burlingame, CA, USA) for 1 hour at room temperature. Sections were then incubated with Vectastain ABC Kit for 1 hour at room temperature, and color was developed using ImmPACT DAB (Vector Laboratories). Hematoxylin was used for counterstaining.

### Imaging of *Dmp1-Cre*-mediated recombination of tdTomato reporter

Hemi-mandibles from 2-month-old *Dmp1-Cre*;*Ai9* mice and *Ai9 Cre*-negative littermates were fixed in 4% PFA in PBS overnight at 4°C with gentle rocking, then decalcified in 10% EDTA.[33] Mandible samples and sections were kept light protected throughout all procedures. The samples were washed in PBS three times at 4°C for 15 minutes with shaking and equilibrated at 4°C in PBS containing 15% sucrose for 4 hours, followed by PBS/30% sucrose overnight as a cryoprotectant. The samples were then embedded in OCT compound for frozen sectioning (Tissue-Tek, Sakura Finetek, Torrance, CA, USA). Seven-micrometer sections were cut on a Leica CM3050S cryomicrotome (Leica Microsystems, Wetzlar, Germany). The sections were stained with DAPI (4 mg/mL in PBS) for 5 minutes at room temperature, then washed three times for 3 minutes with PBS and coverslip mounted using 50% glycerol: 50% PBS:1 mM $MgCl_2$. Sections were fluorescently imaged for tdTomato expression and DAPI using the Keyence (Osaka, Japan) BZ-X800 microscope.

### Fluorochrome labeling and dynamic histomorphometry

Six and 10 days after ligature placement, mice were injected with 200 μL of calcein (10 mg/kg, ip) and 200 μL of alizarin complexone (20 mg/kg, ip). These fluorochromes were diluted with 0.9% NaCl containing 2% NaHCO3. On day 14, maxillae were fixed with 4% PFA for 24 hours, dehydrated with series of ethanol and infiltrated with 50:50 mixture of methyl methacrylate (MMA) and 100% ethanol for 8 hours, 100% MMA for 8 hours, 2 changes of 4% dibutyl phthalate/MMA for 24 hours, then embedded in the plastic (4% dibutyl phthalate 1% perkadox 16/MMA). Samples were cut in the coronal plane at the middle of the second molar using Extec labcut 150 (Extec Corp, Enfield, CT, USA) equipped with a diamond saw (#3030602, UKAM Industrial Superhard Tools, Valencia, CA, USA). The plastic embedded sections were sanded down to achieve 30 to 40 μm thickness (grit no. 320 and 1000). Mineralizing surface per bone surface (MS/BS, %), mineral apposition rate (MAR, μm/d), and bone formation rate (BFR, $\mu m^3/\mu m^2/d$) on the periosteal surface of alveolar bone at the buccal side were measured using ImageJ.

### RNA isolation

Gingival tissues with 1 mm width from the palatal side were used to isolate RNA using Ribozol RNA extraction reagent (VWR Life Science, Radnor, PA, USA). Jawbone tissues including three molars were snap-frozen in liquid nitrogen and crushed into powder using a tissue pulverizer (Cellcrusher Limited, Portland, OR, USA) for RNA extraction. RNA samples from mice without ligature treatment were used for baseline controls for qPCR.

## qPCR analysis

cDNAs were synthesized from 500 ng of total RNA using High-Capacity cDNA Reverse Transcription Kit (Applied Biosystems, Foster City, CA, USA). PowerUP SYBR Green Master Mix (Applied Biosystems, Waltham, MA, USA) was used for qPCR reaction in the QuantStudio 3 (Applied Biosystems). Gene expression levels were calculated using the relative standard curve method. *Hprt* and *Gapdh* were used as internal controls for normalizing target gene expression in in vivo tissue and in vitro cell culture samples, respectively. Primer sequences are listed in Supplemental Table S2.

## Osteoclast locations on alveolar bone tissues

The coordinate of each osteoclast on TRAP-stained alveolar bone sections was recorded using ImageJ. Osteoclast positions relative to bone area were accumulated from the result of six sections and plotted by using R (v 4.0.2).

## Bacterial analysis on ligatures

Silk sutures were recovered from the mouse oral cavity 1 hour, 1 day, 3 days, 5 days, and 7 days after ligature placement. Each suture was vortexed in 500 μL of sterile PBS for 3 minutes. For CFU analysis, bacterial suspension was serially diluted, plated on the blood agar, and incubated for 48 hours in aerobic and anaerobic conditions. Bacterial DNAs isolated from suspensions (Purelink Microbiome DNA Purification Kit, Invitrogen, Waltham, MA, USA) were subjected to 16S rDNA amplicon analysis at BGI America (Cambridge, MA, USA). The V4 region of 16S rDNA was amplified by PCR, and PCR products were used for library construction followed by sequencing and data analysis. Ribosomal Database Project Classifier v. 2.2 was used for taxonomic classification.[34] Qiime2 and R were used to analyze the sequence data.[35]

## Immunofluorescence for peptidoglycans

Paraffin sections were deparaffinized, rehydrated, and incubated with 20 μg/mL of proteinase K (in 50 mM Tris-HCl, 1 mM EDTA, pH 8.0) for 5 minutes at room temperature followed by treatment with 3% $H_2O_2$ for 10 minutes. After blocking of avidin and biotin (Avidin/Biotin Blocking Kit, Vector Laboratories) and mouse IgG (Mouse on Mouse Blocking solution, Vector Laboratories), sections were incubated with anti-peptidoglycan antibody (3F6B3, Bio-Rad) or control mouse IgG at 4°C for overnight, followed by incubation with Mouse on Mouse Biotinylated anti-Mouse IgG reagent for 1 hour at room temperature. Sections were incubated with Streptoavidin-Alexa 574 at room temperature for 1 hour and mounted with an aqueous mounting medium with DAPI.

## Transmission electron microscopy (TEM)

The specimens were fixed with 3% glutaraldehyde/0.1 M cacodylate buffer for 24 to 36 hours at 4°C and then decalcified with 0.5 M EDTA. After the decalcification, specimens were trimmed for the area of interest and post-fixed with 1% osmium tetroxide in cacodylate buffer for 1 hour. The specimens were dehydrated through a series of ethanol and infiltrated with 2 changes of 100% acetone and a 50:50 mixture of acetone and embedding resin (Embed 812, Electron Microscopy Sciences, Hatfield, PA, USA) for 3 days. The specimens were then embedded in resin. Thick sections (1 μm) were cut in the coronal plane until the correct area was determined. Thin sections (80–90 nm) were cut, stained with saturated uranyl acetate in 50% ethanol, and viewed on the Tecnai Spirit. Images were taken with the AMT (Advanced Microscope Techniques, Danvers, MA, USA) CCD camera. The procedures were performed with the support of the Electron Microscopy Core at Indiana University School of Medicine.

## qPCR analysis of bacterial DNA in tissues

DNAs within tissues were isolated from the gingiva (1 mm width) at the palatal side and jawbone. To remove bacteria on the tissue surface, tissues were washed with following procedures: Gingival tissues were sonicated in PBS for 1 minute, then vortexed for 10 seconds. Jawbone tissues were sonicated in 0.3% tween 80/PBS for 1 minute, then vortexed for 10 seconds. The washing step was repeated 3 times by replacing PBS. Gingival tissues were digested with 100 μg/mL proteinase K solution (in 100 mM Tris, 5 mM EDTA, 200 mM NaCl, 0.2% SDS), and DNA was isolated by ethanol precipitation. Jawbone tissues were snap-frozen in liquid nitrogen and crushed into powder using a tissue pulverizer (Cellcrusher Limited) for DNA extraction with proteinase K solution. Tissue DNAs were subjected to qPCR using a primer set targeting bacterial 16S rDNA (337F and 907R) to assess the bacterial load in tissues. 16S rDNA levels were normalized by mouse genomic DNA amplified by primers targeting the mouse *Nod1* gene. Primer sequences are listed in Supplemental Table S3.

## Cell cultures

The MLO-Y4, IDG-SW3, and osteoblast lineage cells from mouse calvaria were used.[28,36,37] MLO-Y4 cells were cultured on plates coated with rat tail type I collagen using α-MEM supplemented with 2.5% fetal bovine serum (FBS), 2.5% calf serum, and 1% penicillin/streptomycin. IDG-SW3 cells were cultured on plates coated with rat tail type I collagen using α-MEM supplemented with 10% FBS, 50 U/mL interferon-gamma, and 1% penicillin/streptomycin at 33°C until they become confluent completely. IDG-SW3 cells were further cultured with osteogenic induction medium (α-MEM supplemented 10% FBS, 1% penicillin/streptomycin, 5 mM β-glycerophosphate, and 50 μg/mL ascorbic acid) at 37°C for 4 and 28 days to obtain osteoblastic and osteocytic cells, respectively. Calvarial osteoblast-enriched cells (Ob) and osteocyte-enriched cells (Ocy) were isolated as we have performed previously.[28] Cells were stimulated with C14-Tri-LAN-Gly (InvivoGen, San Diego, CA, USA). For siRNA-mediated knockdown, MLO-Y4 cells were seeded at the density of $2.0 \times 10^3$ cells/cm$^2$ on either 6-well or 12-well plates. After 24 hours, siRNA for *Ikk1*, *Ikk2*, *Jnk1*, *Jnk2*, *Mek1*, *Mek2*, *p38α*, *p38β*, *p38γ*, *c-Fos*, *Stat3*, *Stat5*, *Creb1*, *Runx2*, and scramble siRNA (Santa Cruz Biotechnology) were transfected using TransIT-X2 Dynamic Delivery System (Mirus Bio, Madison, WI, USA). After 48 to 72 hours of siRNA transfection, cells were stimulated with C14-Tri-LAN-Gly for 3 hours and lysed for RNA isolation.

## Macrophage isolation

Bone marrow cells were collected from tibias and femurs of 10-week-old mice. After the removal of red blood cells with RBC lysis buffer, bone marrow cells were incubated with α-MEM supplemented with 10% FBS and 1% penicillin/streptomycin for 3 hours on petri dishes to allow stromal cells

to adhere to the dishes. Non-adherent cells were collected and seeded on culture dishes at a density of $5.0 \times 10^4$cells/cm$^2$ well and incubated in the presence of macrophage colony-stimulating factor (M-CSF; 25 ng/mL, PeproTech, Rocky Hill, NJ, USA) for 2 days to obtain bone marrow-derived M-CSF-dependent macrophages.

### Western blotting

MLO-Y4 cells stimulated with C14-Tri-LAN-Gly or vehicle were lysed with lysis buffer (1% Triton X-100, 25 mM Tris-HCl (pH 7.4), 150 mM NaCl, 5 mM EDTA, 10% glycerol, 2.5 mM sodium pyrophosphate, 0.7 mM β-glycerophosphate) supplemented with protease and phosphatase inhibitor cocktails (Sigma-Aldrich, St. Louis, MO, USA). Five micrograms of protein samples were resolved by SDS-PAGE under reducing conditions and transferred to nitrocellulose membranes. After blocking with 5% skim milk in TBS solution supplemented with 1% Tween-20, membranes were incubated with anti-phospho-IKKα/β (Cell Signaling Technology, Danvers, MA, USA; #2697), anti-IKKβ (#8943), anti-phospho-p38 (#4511), anti-p38 (#8690), anti-phospho-ERK (#4370), anti-ERK (#4695), anti-phospho-JNK (#4668), anti-JNK (#9258), anti-phospho-c-Fos (#5348), anti-c-Fos (#2250), or anti-Actin (Santa Cruz, C4, sc-47778) antibody overnight at 4°C followed by incubation with HRP-conjugated secondary antibodies (Cell Signaling Technology, #7074 or 7076). Bands were detected using SuperSignal West Dura or Femto chemiluminescent substrates (Thermo Fisher Scientific, Waltham, MA, USA) and visualized by using the Celvin S320 Imager (Biostep, Burkhardtsdorf, Germany). Immunoblotting images with molecular weight markers are presented in Supplemental Figure S14.

### Statistics

The two-tailed unpaired Student's *t*-test was used to compare means between two groups. One-way ANOVA with the Tukey–Kramer post hoc test was used to compare means among three or more groups. $p < 0.05$ was considered significant. GraphPad (La Jolla, CA, USA) Prism software was used for statistical analysis. Male and female groups were analyzed independently to detect sexual dimorphisms.

## Results

### LIP induces tooth displacement and bone formation in addition to bone resorption

To understand the temporal dynamics of alveolar bone-tooth interaction and alveolar bone resorption in LIP, μCT analysis was performed at eight time points over 14 days. As the parameters, the width of the PDL space at the apical root, the total distance between the CEJ and the ABC, the BV, and the BV/TV between two buccal roots of the maxillary second molar were measured (Supplemental Fig. S1*A*, *B*). Mice with tooth root fusion on either the ligated or unligated side were excluded from the analysis because of difficulties in normalizing BV loss (Supplemental Fig. S1*C*–*E*). Although alveolar bone erosion became evident from day 5 (Fig. 1*A*, yellow arrowheads), we unexpectedly identified the expansion of the PDL space at day 1 (Fig. 1*A*, a white arrowhead) and detected woven bone formation on the alveolar surface from day 7 (Fig. 1*A*, blue arrowheads). Contrary to the dogma that the ABC is the primary site of bone loss in periodontitis, bone loss occurred throughout the alveolar bone area (Fig. 1*A*). H&E staining of the PDL area on day 1 revealed an increase in the intercellular space accompanied by edematous changes of the PDL tissue and infiltration of neutrophils/monocytes and macrophages (Fig. 1*B* and Supplemental Fig. S2). The increase in CEJ-ABC distance was enhanced after day 7, suggesting that tooth displacement due to expansion of the PDL space, but not osteoclast induction, is responsible for the small increase in CEJ-ABC distance between days 1 and 5. Alveolar BV loss peaked on day 7, and the significant BV loss on day 5 preceded the enhanced increase in CEJ-ABC distance on day 7. Interestingly, BV loss was restored on days 10 and 14. Accordingly, BV/TV started to decrease from day 5 and reached its lowest value on day 7. However, it recovered significantly thereafter (Fig. 1*C* and Supplemental Fig. S3*A* for female data). In contrast, the increase in CEJ-ABC distance was maintained until day 14. Next, to investigate the mechanism of how bone loss recovers after day 10, we utilized double fluorochrome labeling of the alveolar bone.[38] Incorporation of fluorochrome dyes was observed in broad areas of the alveolar bone, including the ABC and the endosteal and periosteal sides of the alveolar bone (Fig. 1*D*, boxes a, b, and c, respectively). Fluorescence signals were stronger on the ligated side than on the unligated side. Dynamic histomorphometric analysis revealed that MS/BS, MAR, and BFR were all significantly higher in the ligated alveolar bone (Fig. 1*E* and Supplemental Fig. S3*B* for female data), indicating that the bone formation is stimulated in LIP and that the increase in bone formation contributes to the restoration of BV/TV by day 14. Consistent with these data, osteoblast surface/bone surface (Ob.S/BS) and alkaline phosphatase activity were increased after ligature placement with osteoid formation (Supplemental Fig. S4*A*–*E*). Although ligature placement downregulated the expression of osteoblast-associated genes on day 1, these expression levels increased by day 7 compared with day 1 (Supplemental Fig. S4*F*). Bone formation even at the ABC region suggested that the increased CEJ-ABC distance in the LIP model is the net effect of bone formation and resorption. Taken together, our data show that LIP not only induces alveolar bone resorption/erosion but also causes tooth displacement and strong bone formation in a disease stage-specific manner. Furthermore, our data indicate that 3D BV analysis is more sensitive than 1D CEJ-ABC analysis in assessing alveolar bone loss in LIP mice.

### Osteoclast induction is transient and occurs across the entire alveolar bone surface in LIP

We next examined if osteoclast induction is affected by the location on the alveolar bone and if it changes in a stage-specific manner in LIP. Histomorphometric analysis revealed that TRAP-positive osteoclasts were induced throughout the alveolar bone (Fig. 2*A*), demonstrating that the ABC is not necessarily the primary site of osteoclast induction during the LIP process. The absence of TRAP-positive osteocytes in alveolar bone suggested that osteocytic osteolysis is unlikely to be induced by LIP. The N.Oc/BA was transiently increased on days 3, 5, and 7 and then decreased, whereas the increases in osteoclast surface/bone surface (Oc.S/BS) and number of osteoclasts/bone surface (N.Oc/BS) peaked on days 3 and 5 (Fig. 2*B* and Supplemental Fig. S5 for female data). The temporal increase in osteoclast induction was confirmed by the temporal upregulation of osteoclast marker genes in the jawbone (Fig. 2*C*). The transient increases in *Rankl* and *Rankl*/*Opg* ratio in the jawbone on day 1 before osteoclast induction confirms that osteoclasts are induced in a stage-specific manner in the LIP model (Fig. 2*D*). The IL-1β, IL-6, TNF-

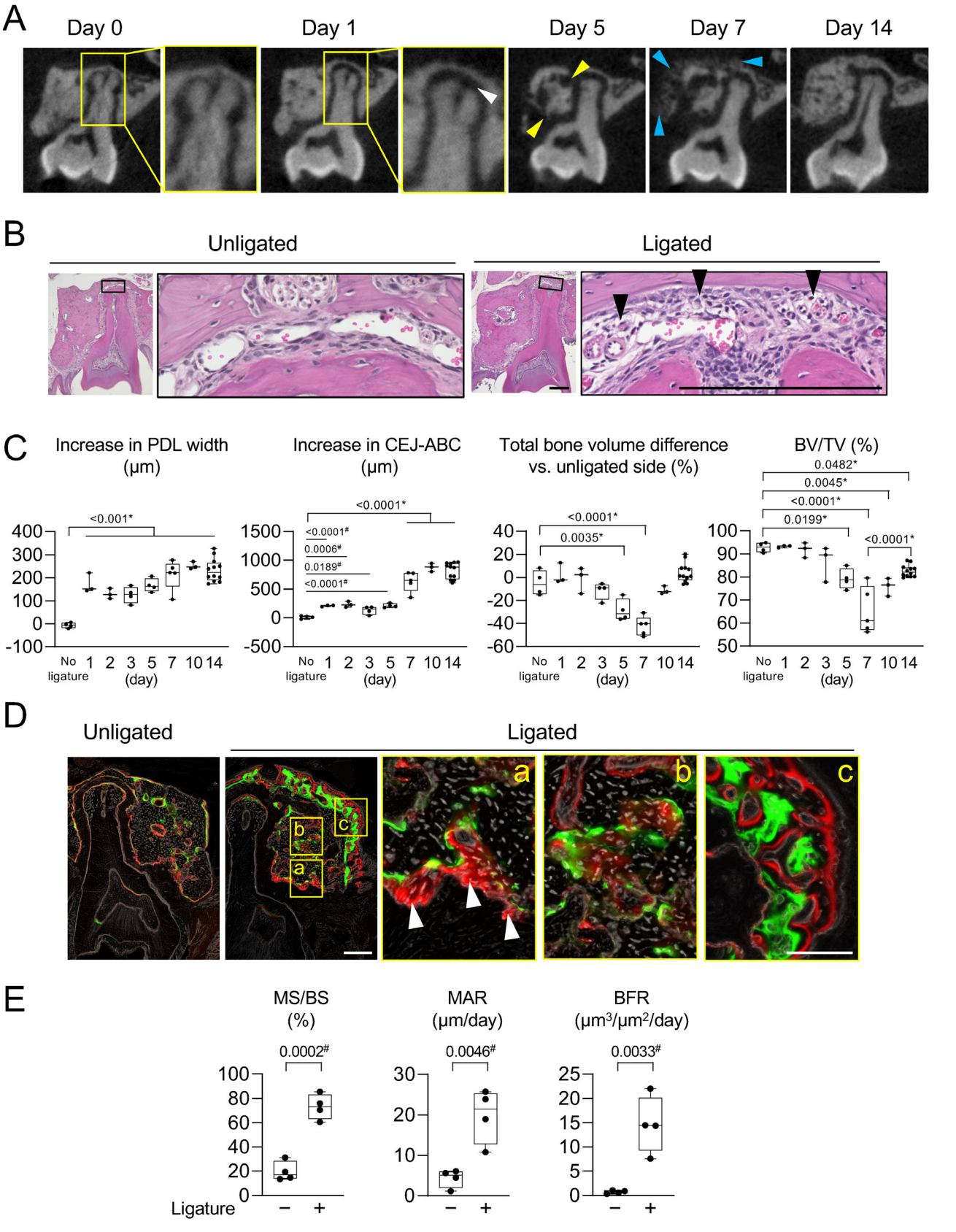


*(Figure legend continues on next page.)*

α, and IL-17 cytokines are known to regulate inflammation and osteoclastogenesis in periodontitis.[39-43] Similar to the *Rankl* induction pattern, *Il1b* and *Il6* in gingival tissues increased sharply on day 1, whereas *Il17a* did not increase significantly until day 14 (Fig. 2*E*). No upregulation of *Tnf* or *Il17f* was observed during the LIP process (Fig. 2*E*). The rapid accumulation of neutrophils/monocytes in gingival tissues by day 1 indicates that inflammatory cells are involved in the sharp and strong induction of *Il1b* and *Il6* in the gingiva (Supplemental Fig. S6). These data suggest that the strong but transient innate immune activation in the early phase contributes to the induction of transient osteoclastogenesis in LIP, but unlike previous findings,[11,12,17] adaptive immune responses may have a limited impact on the induction of osteoclasts in our LIP experimental conditions. To confirm that increased osteoclast formation is responsible for bone resorption in LIP, we treated the LIP mice with zoledronic acid (ZA). ZA treatment significantly protected against alveolar BV loss and osteoclast induction (Supplemental Fig. S7*A–D*). In contrast, the increase in PDL space width was not inhibited by ZA treatment (Supplemental Fig. S7*E*). Accordingly, the small increase in CEJ-ABC distance before day 7 was equivalent between the ZA and vehicle treatment groups (Supplemental Fig. S7*F*), suggesting that tooth displacement occurs independently of osteoclast activity. Taken together, these results indicate that the osteoclast induction identified throughout the alveolar bone region and gingival inflammation occur in a stage-dependent manner in LIP and that osteoclasts drive alveolar bone resorption in the LIP model.

## Antibiotics treatment suppresses alveolar bone loss, osteoclastogenesis, gingival inflammation, and edematous changes of PDL

Consistent with previous studies,[6,7,30] antibiotics treatment starting from 5 days before ligature placement protected against alveolar bone resorption and osteoclast induction in our LIP mice (Fig. 3*A, B* and Supplemental Fig. S8*A, B* for female data). It also suppressed *Rankl* levels and *Rankl/Opg* ratio in jawbone tissues and inhibited inflammatory cytokine gene expression in the gingiva (Fig. 3*C*). Accordingly, bone formation on the periosteal surface was reduced in LIP mice treated with antibiotics (data not shown). Antibiotics treatment also prevented the increase in PDL space (Fig. 3*D* and Supplemental Fig. S8*C* for female data) and edematous changes of periodontal ligament cells (Fig. 3*E*), which were accompanied by a reduction in inflammatory cell infiltration (Fig. S8*D*). These data support the essential role of oral commensal bacteria in driving LIP phenotypes, including jawbone destruction, tooth displacement, and gingival inflammation.

## LIP induces bacterial invasion into the periodontal soft tissue and bone

To examine the association of bacterial load with alveolar bone loss and osteoclastogenesis in LIP, we quantified bacterial colony-forming unit (CFU) and characterized the bacterial composition in silk sutures. The CFUs of both aerobic and anaerobic bacteria increased in a time-dependent manner (Supplemental Fig. S9*A*). 16S rDNA analysis revealed that the bacterial composition changed dramatically between 1 and 24 hours after ligature placement but showed similar compositions after 24 hours (Supplemental Fig. S9*B*). These results indicate that bacterial load reaches the maximum and oral dysbiosis is established before the completion of alveolar bone loss in LIP. Furthermore, these data imply that changes in bacterial composition are associated with the initiation of gingival inflammation. Immunofluorescence staining revealed that LIP facilitated the dissemination of bacterial peptidoglycans to the gingival connective and periodontal ligament tissues on day 1, although peptidoglycans were restricted to the junctional epithelial tissues before LIP induction (Fig. 4*A*). To further characterize the bacterial dissemination, transmission electron microscopy (TEM) analysis was performed. We identified bacteria invaded gingival and periodontal ligament tissues (Fig. 4*B*). Bacterial invasion even into the osteocyte lacunar system of alveolar bone was observed after LIP (8 of 52 lacunar spaces, Fig. 4*B*). qPCR analysis of 16S rDNA showed that the bacterial load in the gingival tissue was increased on day 1 and decreased thereafter (Fig. 4*C*), which correlated with the increase of *Il1b* and *Il6* in the gingiva. The LIP-induced bacterial dissemination was blocked by antibiotics treatment (Supplemental Fig. S9*C, D*). The bacterial composition within gingival tissues appeared to be different before and after LIP (Fig. 4*D*). TEM analysis revealed neutrophil infiltration into gingival and periodontal ligament tissues (Supplemental Fig. S9*E*, yellow arrowheads), indicating that bacteria clearance by these inflammatory cells may be involved in the mechanism of bacterial load reduction after day 1. In contrast, the bacterial load in the jawbone did not decrease after day 1 (Supplemental Fig. S9*F, G*), suggesting that these phagocytes cannot easily access the osteocyte lacunar space.

## T/B lymphocytes are not required for bone loss in LIP

T and B cells are known to play critical roles in the development of periodontitis and alveolar bone loss.[11,12,44-46] However, our gene expression analysis (Fig. 2*E*) and a previous study[14] showed that the expression of adaptive immunity-associated genes peaked after the establishment of osteoclast induction,

*(Figure legend continued from previous page.)*

**Fig. 1.** Time-course characterization of the ligature-induced periodontitis (LIP) model. (*A*) Two-dimensional μCT images at the middle of the second molar in the coronal plane. A white arrowhead = expanded periodontal ligament (PDL) space; yellow arrowheads = bone eroded regions; blue arrowheads = bone formation on the periosteal surface. (*B*) H&E staining of the PDL tissues underneath the palatal tooth root of the maxillary second molar 1 day after LIP treatment. Arrowheads indicate increased intercellular spaces. Scale bar = 200 μm. (*C*) Quantitative analysis of the PDL width, cementoenamel junction-alveolar bone crest (CEJ-ABC) distance, alveolar bone volume (BV), and alveolar BV/trabecular volume (TV) using μCT. (*D*) Fluorescent microscopic images of jawbones from mice with or without ligatures administrated with calcein (day 6, green) and alizarin complexone (day 10, red). Coronal plane images were taken at day 14. Arrowheads indicate newly mineralized regions at ABC. Scale bar = 200 μm in lower magnification and 100 μm in higher magnification. (*E*) Dynamic histomorphometry analysis to assess bone formation. MS/BS = mineralized bone surface per bone surface; MAR = mineral apposition rate; BFR = bone formation rate. (*A–E*) Data from wild-type male mice. $^{\#}p < 0.05$ by Student's *t*-test. $^{*}p < 0.05$ by one-way ANOVA with Tukey–Kramer test.

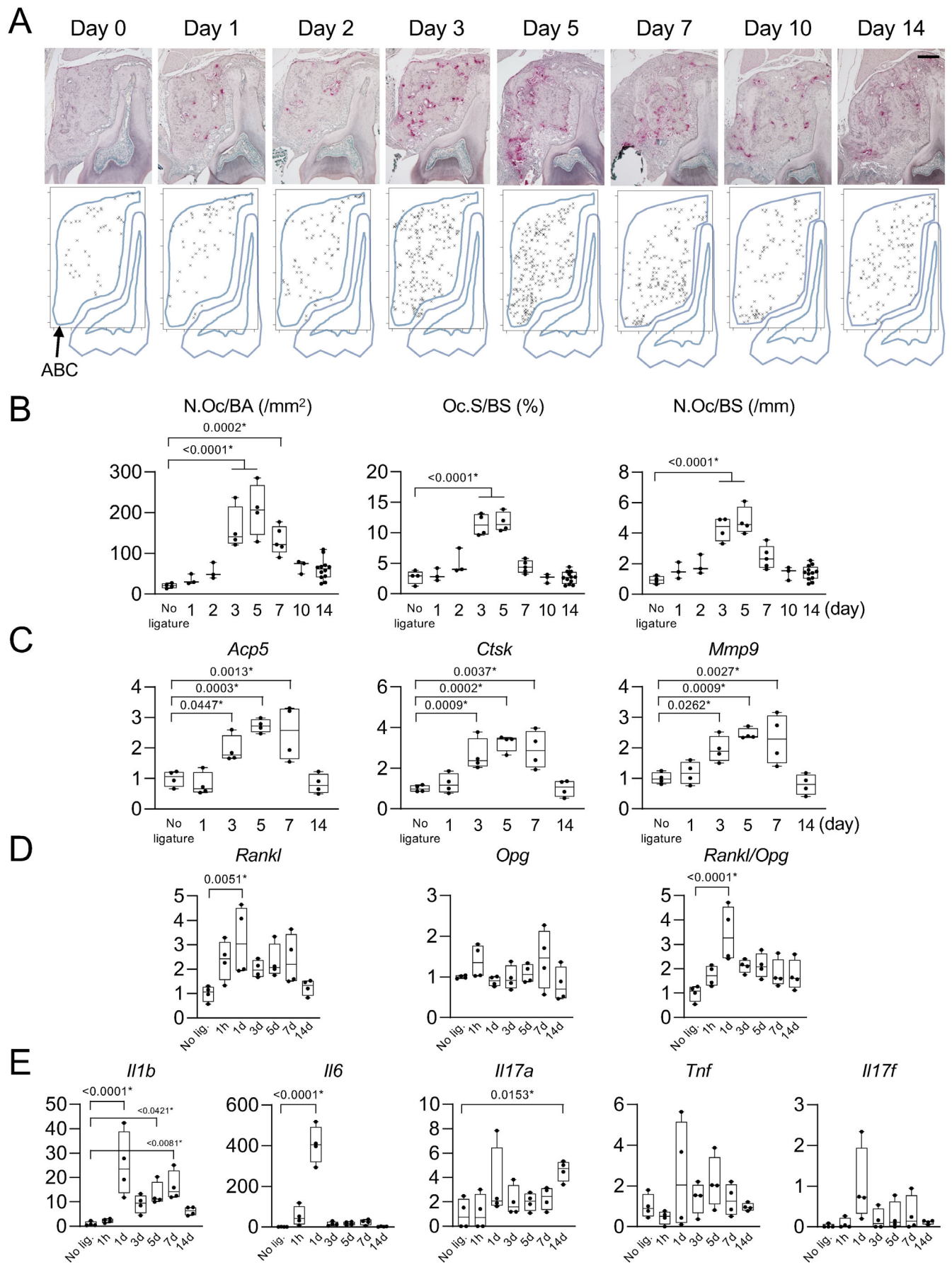


*(Figure legend continues on next page.)*

suggesting that T/B lymphocytes may not be critical for osteoclast induction in LIP. To investigate whether these cells are required for osteoclastic bone loss in the LIP model, we used RAG1-deficient mice lacking T/B cells.[47] Remarkably, the absence of T/B lymphocytes did not decrease the bone loss or osteoclast induction in LIP (Fig. 5*A, B* and Supplemental S10*A, B* for female data). In agreement with these results, *Rankl* levels in the jawbone were not decreased in RAG1-deficient mice challenged with LIP (Fig. 5*C* and Supplemental S10*C* for female data). These results demonstrate that osteoclastic bone loss can be induced in the absence of T/B lymphocytes in LIP and suggest that T/B lymphocytes are not the major source of RANKL in LIP mice.

## Osteocytes are a major source of RANKL to induce osteoclasts in LIP

Osteocytes are the terminally differentiated cells of the osteoblastic lineage embedded in the bone matrix.[48] They are the most abundant cells in the bone and are known to be a major source of RANKL in physiological bone remodeling as well as in *Pg*-induced periodontitis in mice.[20,23,24,28,49] However, despite these facts, it remains unknown whether osteocytes provide RANKL for osteoclast formation in LIP. To study the effect of osteocyte RANKL in LIP, *Dmp1-Cre;Rankl*$^{fl/fl}$ mice lacking RANKL in osteocytes and mature osteoblasts, but predominantly in osteocytes, were generated.[28] Tooth eruption was normal in the *Dmp1-Cre;Rankl*$^{fl/fl}$ mice. Since a previous report showed that osteoblasts and PDL cells are major sources of RANKL in the LIP model,[12] we first investigated whether *Dmp1-Cre*-mediated DNA recombination occurs in these cells in addition to osteocytes by using *Dmp1-Cre;Ai9* mice. *Dmp1-Cre* induced gene recombination in osteocytes and mature osteoblasts but not in cells of the PDL (Fig. 6*A* and Supplemental Fig. S11 for female data). Next, we challenged the *Dmp1-Cre;Rankl*$^{fl/fl}$ mice with LIP and found that deletion of RANKL in osteocytes and mature osteoblasts significantly blocked alveolar bone loss (Fig. 6*B, C* and Supplemental Fig. S12*A* for female data). To examine the impact of osteoblast-derived RANKL in LIP, *Col1a1-Cre*$^{ERT2}$*;Rankl*$^{fl/fl}$ mice were generated and challenged with LIP after administration of tamoxifen for 5 consecutive days followed by a 2-day interval.[31,50] These mice exhibited bone loss comparable to control mice (Supplemental Fig. S12*B*), suggesting that osteoblasts are not a major source of RANKL in LIP. The *Dmp1-Cre;Rankl*$^{fl/fl}$ mice on the RAG1-deficient background showed that RANKL from osteocytes and mature osteoblasts controls bone loss in LIP even in the absence of T/B lymphocytes (Fig. 6*D* and Supplemental Fig. S12*C* for female data). Consistent with these results, osteoclast induction and *Rankl* expression were suppressed in *Dmp1-Cre;Rankl*$^{fl/fl}$ mice challenged with LIP (Fig. 6*E*–*G* and Supplemental Fig. S12*D, E* for female data). Considering our recent finding that *Dmp1-Cre* deletes RANKL predominantly in osteocytes rather than in osteoblasts, and the fact that osteocytes are the most abundant cell type in bone,[28,48] these data suggest that osteocytes, rather than osteoblasts and PDL cells, are a major source of RANKL in LIP to regulate bone resorption.

## Activation of the NOD1 pathway induces *Rankl* in osteocytes

Osteoblast lineage cells have been shown to upregulate RANKL expression in response to pro-inflammatory cytokines and bacterial PAMPs.[29,51-56] Recently, we have shown that direct stimulation of osteocytes via TLR2 and TLR4 by bacterial PAMPs induces RANKL expression significantly higher than in osteoblasts and that the TLR2-RANKL axis in osteocytes regulates alveolar bone resorption in periodontitis caused by *Pg*.[28] Therefore, we hypothesized that activation of TLR2/4 signaling pathways is involved in the mechanism of bone resorption in LIP. However, no protection against bone loss was observed in mice defective in both TLR2 and TLR4 pathways (Fig. 7*A* and Supplemental Fig. S13*A* for female data). Consistent with this result, mice deficient in MYD88, an adaptor protein essential for signaling activation by all TLRs except TLR3,[57] developed bone loss comparable to control mice (Fig. 7*B* and Supplemental Fig. S13*B* for female data), suggesting that TLR signaling pathways are not critical for inducing bone loss in LIP. A previous study reported that activation of NOD1, a pattern recognition receptor (PRR) for peptidoglycans from Gram-positive and Gram-negative bacteria, is responsible for bone loss in LIP.[30] We found that MLO-Y4 cells,[36] IDG-SW3 cells[37] in the osteocytic phase (day 28), and osteocyte- and osteoblast-enriched cell populations from mouse calvaria (Ocy and Ob, respectively)[28] expressed NOD1 protein at levels higher than or comparable to mouse bone marrow-derived M-CSF-dependent macrophages (Fig. 7*C*). To determine whether activation of osteocytes via the NOD1 pathway induces *Rankl* expression, these cells were stimulated with a synthetic NOD1 agonist, C14-Tri-LAN-Gly (C14). C14 treatment significantly promoted *Rankl* expression in all osteocytic cells but not in Ob (Fig. 7*D*). In agreement with our recent report using TLR agonists, osteocytic IDG-SW3 cells and Ocy were significantly more responsive to C14 than osteoblastic IDG-SW3 cells and Ob, respectively, to express *Rankl* (Fig. 7*D*). Mechanistically, C14 stimulation of MLO-Y4 cells induced the phosphorylation of IKKα/β, p38, ERK, JNK, and c-Fos, which are known to mediate the activation of the NOD1 signaling pathway (Fig. 7*E*). Interestingly, NOD1 stimulation caused a markedly sharp and strong induction of c-Fos protein and mRNA at 1 hour (Fig. 7*E* and Supplemental S13*C*). Knockdown of *Ikk1/2*, *p38α/β/γ*, or *c-Fos* by siRNA significantly suppressed C14-induced *Rankl* induction in MLO-Y4 cells (Fig. 7*F* and Supplemental Fig. S13*D*), suggesting the involvement of these signaling pathways in the mechanism of *Rankl* induction downstream of NOD1. Knockdown of *Jnk1/2* or *Mek1/2* failed to downregulate *Rankl* expression. Furthermore,

*(Figure legend continued from previous page.)*

**Fig. 2.** Time-course analysis of osteoclast induction in the ligature-induced periodontitis (LIP) model. (*A*) Upper images: tartrate-resistant acid phosphatase (TRAP) staining of the jawbone tissues underneath the second molar with ligatures. Coronal plane images. Scale bar = 200 μm. Lower images: Relative positions of osteoclasts on TRAP-stained sections. Osteoclast positions were results from 6 sections at each time point. ABC = alveolar bone crest. (*B*) Histomorphometry for osteoclasts on the alveolar bone underneath the ligated second molar. (*C*) qPCR analysis of osteoclast-associated gene levels in jawbone tissues normalized by *Hprt*. (*D*) qPCR analysis of *Rankl*, *Opg*, and *Rankl/Opg* ratio in the jawbone tissues normalized by *Hprt*. (*E*) Inflammatory gene expression levels in the gingival tissues normalized by *Hprt*. (*A*–*E*) Data from wild-type male mice. *$p < 0.05$ by one-way ANOVA with Tukey–Kramer test.

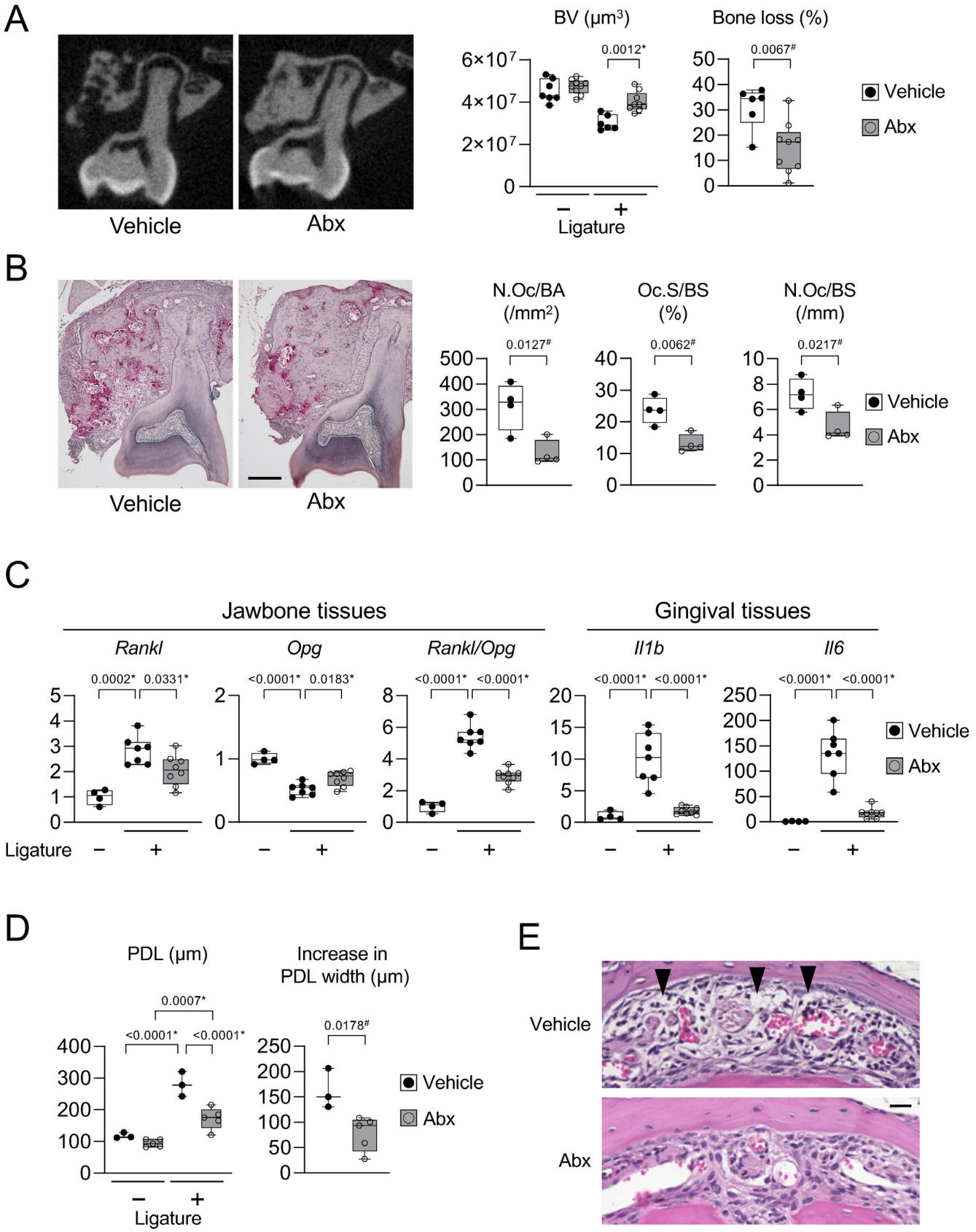


*(Figure legend continues on next page.)*

knockdown of *Creb1*, *Runx2*, *Stat3*, or *Stat5*, transcription factors that regulate *Rankl* transcription in osteoblast lineage cells,[58] did not suppress C14-induced *Rankl* induction in MLO-Y4 cells (Supplemental Fig. S13*E*). Thus, NOD1 is highly expressed in osteocytes, and activation of the NOD1 pathway upregulates *Rankl* expression in osteocytes via NF-kB, p38, and c-Fos, suggesting that the NOD1-RANKL axis in osteocytes may be a key mechanism for the induction of osteoclastogenesis and alveolar bone resorption in the LIP model.

## Discussion

The mouse LIP model has been widely used to elucidate the pathogenesis of human periodontitis. Because of its rapid and reproducible initiation of bone resorption upon ligature placement, the LIP model has been regarded as a model to primarily investigate the mechanism of bone resorption in relation to gingival tissue inflammation, immune cell activation, and oral dysbiosis. Notably, our careful evaluation of alveolar bone revealed that both alveolar BV loss and osteoclast induction are more transient and dynamic than we thought and that they return to normal levels even when silk sutures remain ligated. Increased osteoclastogenesis was found to precede BV loss and an increase in the CEJ-ABC distance. Thus, transient elevation of *Rankl* and certain types of inflammatory cytokines in periodontal tissues may be a cause of transient osteolysis in LIP. Although the bacterial load in ligatures remains high, their invasion into gingival tissues changes dynamically during LIP. Because LIP depends on the presence of oral bacteria, mechanisms of bacterial invasion and clearance in periodontal tissues will need to be investigated to understand the time-dependent regulation of the expression of cytokines, including RANKL, and bone resorption in the LIP model. Osteocyte activation by oral bacteria may contribute to the process.

Our TEM analysis identified bacterial particles in approximately 15% of the lacunae in LIP. However, it remains unclear whether "direct bacteria-osteocyte interactions" are required for bone resorption in LIP. Alternatively, it would be reasonable to assume that osteocytes do not necessarily need to be stimulated by live bacteria in the LIP, given the diameter of the canaliculi, the most expected routes for live bacteria to access osteocytes. We believe that PAMPs, such as peptidoglycans released by oral bacteria, are more important to stimulate osteocyte PRRs to induce RANKL in the pathogenesis of periodontitis including LIP. Further studies are needed to determine the detailed mechanism of how oral microorganisms and their PAMPs reach the alveolar bone osteocytes in LIP. Although it remains to be determined whether oral bacteria directly interact with osteocytes in human periodontitis, human periodontitis can cause osteomyelitis in the jaw[59,60] and bacteria-osteocyte interactions have been suggested in human and mouse osteomyelitis.[61-63] In addition, it would be interesting to investigate how osteocytes behave after interacting with live bacteria and their PAMPs during periodontitis, besides promoting RANKL expression (eg, cell damage and death, engulfment of bacteria, or secretion of inflammatory mediators).

It was unknown whether LIP induces bone formation and can be used as a model to study the impact of osteoblast activation in periodontitis. Surprisingly, we identified a significant increase in bone formation after the bone resorption phase, suggesting that restoration of bone volume is due, at least in part, to alveolar bone formation and that BV changes in LIP are the net result of bone resorption and bone formation. Osteoblast activation might mask the osteoclastic bone resorption in LIP analysis depending on the time points. Thus, we propose that LIP is a valuable model for studying the role of osteoblasts in periodontitis. Unexpectedly, we also discovered that the width of the PDL increases after ligature placement, which affects the measurement of the total CEJ-ABC distance. These results suggest that careful selection of the time points would be critical for LIP analysis depending on parameters. In other words, analysis at multiple time points would be preferred to assess the LIP phenotypes comprehensively.

Decreases in BV were detected earlier than increases in the CEJ-ABC distance, suggesting that 3D BV analysis is more sensitive than 2D CEJ-ABC analysis for detecting bone loss. Similarly, in human patients, BV analysis with CT may detect more subtle and earlier changes in alveolar bone loss that may be overlooked by CEJ-ABC distance measurement. The CEJ-ABC distance has been the gold standard parameter for assessing alveolar bone loss in human and animal periodontitis. One of the main reasons for this would be the assumption that the ABC is the primary site of bone resorption in periodontitis. However, our study showed that LIP-induced osteoclast formation is widely distributed throughout the alveolar bone area, which is also the case in the *Pg*-induced periodontitis model,[28] and that there is no evidence showing that ABC is the primary site of increased osteoclast formation in the LIP model. The wide distribution of osteoclast induction is also likely to be the case in human periodontitis.[64] Furthermore, the fact that the decrease in BV precedes the increase in the CEJ-ABC distance supports the idea that ABC is not necessarily the exclusive site of bone resorption analysis in LIP. Bone formation at the ABC, as demonstrated by fluorochrome labeling, suggests that the CEJ-ABC distance may also be influenced by osteoblast activity in LIP. However, in human periodontitis, it remains unclear whether osteoclasts are induced throughout the alveolar bone and whether and where bone formation is stimulated in the alveolar bone. Histomorphometric analysis of bone samples from human periodontitis patients would be necessary.

*(Figure legend continued from previous page.)*

**Fig. 3.** Bacteria-dependent osteoclast induction, alveolar bone loss, and periodontal ligament (PDL) responses in the ligature-induced periodontitis (LIP) model. (*A*) Left: Two-dimensional μCT images at the middle of the second molar in the coronal plane. Right: μCT analysis of the alveolar bone volume and percentage of alveolar bone volume loss induced by LIP. (*B*) Left: TRAP staining of the jawbone tissues sectioned in the coronal plane. Scale bar = 200 μm. Right: Histomorphometry for osteoclasts on the alveolar bone underneath the ligated second molar. (*C*) qPCR analysis of osteoclast-associated genes in the jawbone and inflammatory genes in the gingiva. *Hprt* was used for normalization. (*D*) PDL width after LIP treatment. (*E*) H&E staining of the PDL tissues underneath the buccal tooth root of the maxillary second molar with and without ligatures. Arrowheads indicate the increased intercellular spaces. Scale bar = 20 μm. (*A–E*) Data from wild-type male mice. (*A, B*) Five days after LIP treatment. (*C–E*) One day after LIP treatment. $^{\#}p < 0.05$ by Student's *t*-test. $^{*}p < 0.05$ by one-way ANOVA with Tukey–Kramer test. Abx = antibiotics cocktail.

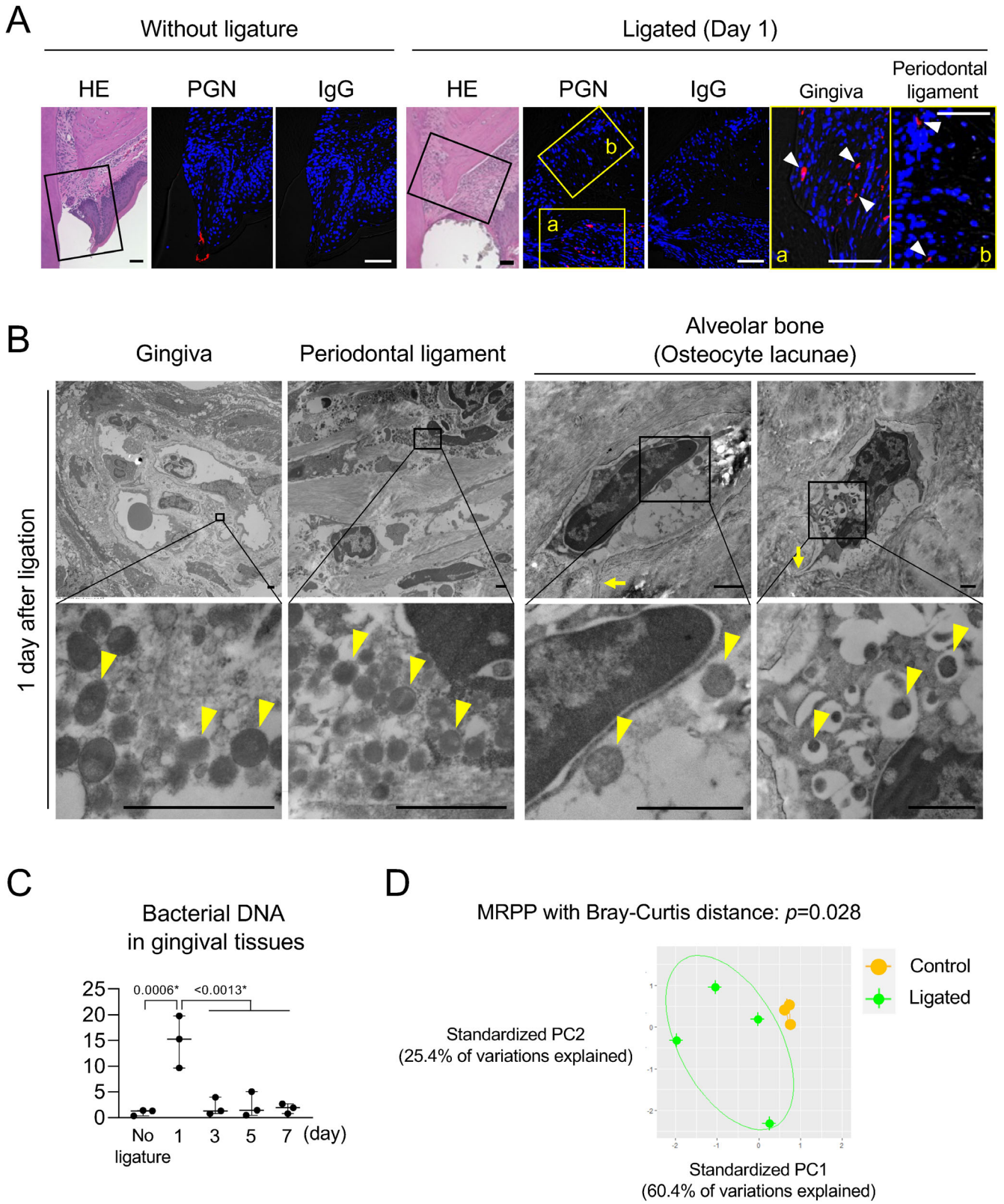


**Fig. 4.** Bacterial invasion into periodontal tissues and the osteocyte lacunar system in the ligature-induced periodontitis (LIP) model. (*A*) H&E staining of periodontal tissues and immunohistochemical staining of peptidoglycan in periodontal tissues. PGN = peptidoglycan (red). Nuclei were visualized by DAPI (blue). Arrowheads indicate the location of PGN. Scale bar = 50 μm. (*B*) Transmission electron microscopy (TEM) analysis at day 1 after LIP induction. Scale bar = 1 μm. Arrowheads indicate bacterial particles. Arrows indicate the canaliculi. (*C*) Relative amounts of 16S rDNA in the gingival tissues analyzed by qPCR. The average of 16S rDNA levels in the gingival tissues from mice without ligatures was set as 1. (*D*) Principal component analysis (PCA) and multi-response permutation procedure (MRPP) with Bray–Curtis distance analyses of 16S rDNA isolated from the gingival tissues. (*A–D*) Data from wild-type male mice. *$p < 0.05$ by one-way ANOVA with Tukey–Kramer test.

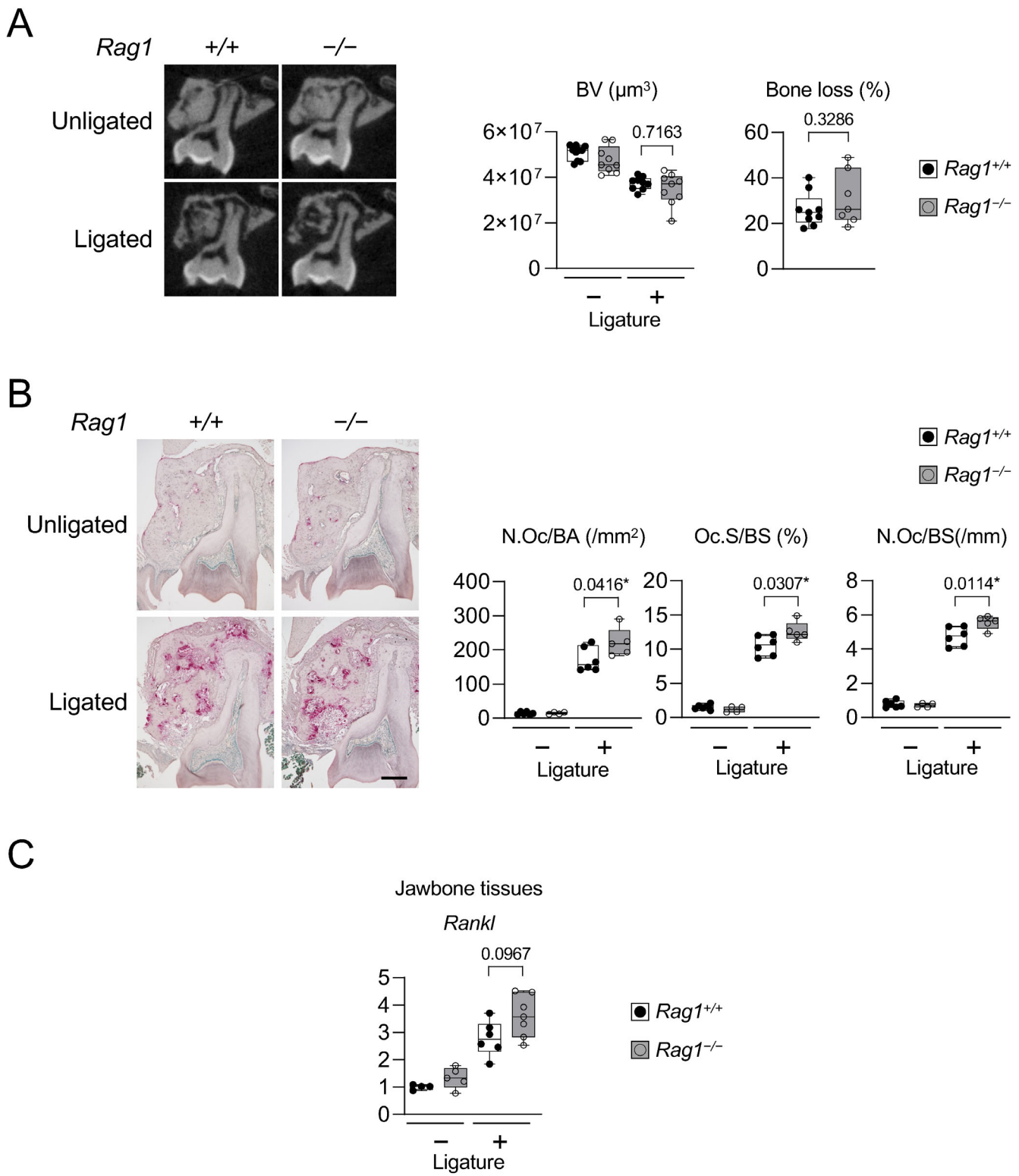


**Fig. 5.** No requirement of T/B lymphocytes for osteoclast induction and alveolar bone loss in the ligature-induced periodontitis (LIP) model. (*A*) Left: Two-dimensional μCT images at the middle of the second molar in the coronal plane. Right: μCT analysis of the alveolar bone volume and percentage of alveolar bone volume loss induced by LIP. (*B*) Left: TRAP staining of the jawbone tissues sectioned in the coronal plane. Scale bar = 200 μm. Right: Histomorphometry for osteoclasts on the alveolar bone underneath the ligated and unligated second molar. (*C*) qPCR analysis of *Rankl* in the jawbone tissues normalized by *Hprt*. (*A–C*) Five days after LIP treatment. Data from male mice. *$p < 0.05$ by one-way ANOVA with Tukey–Kramer test.

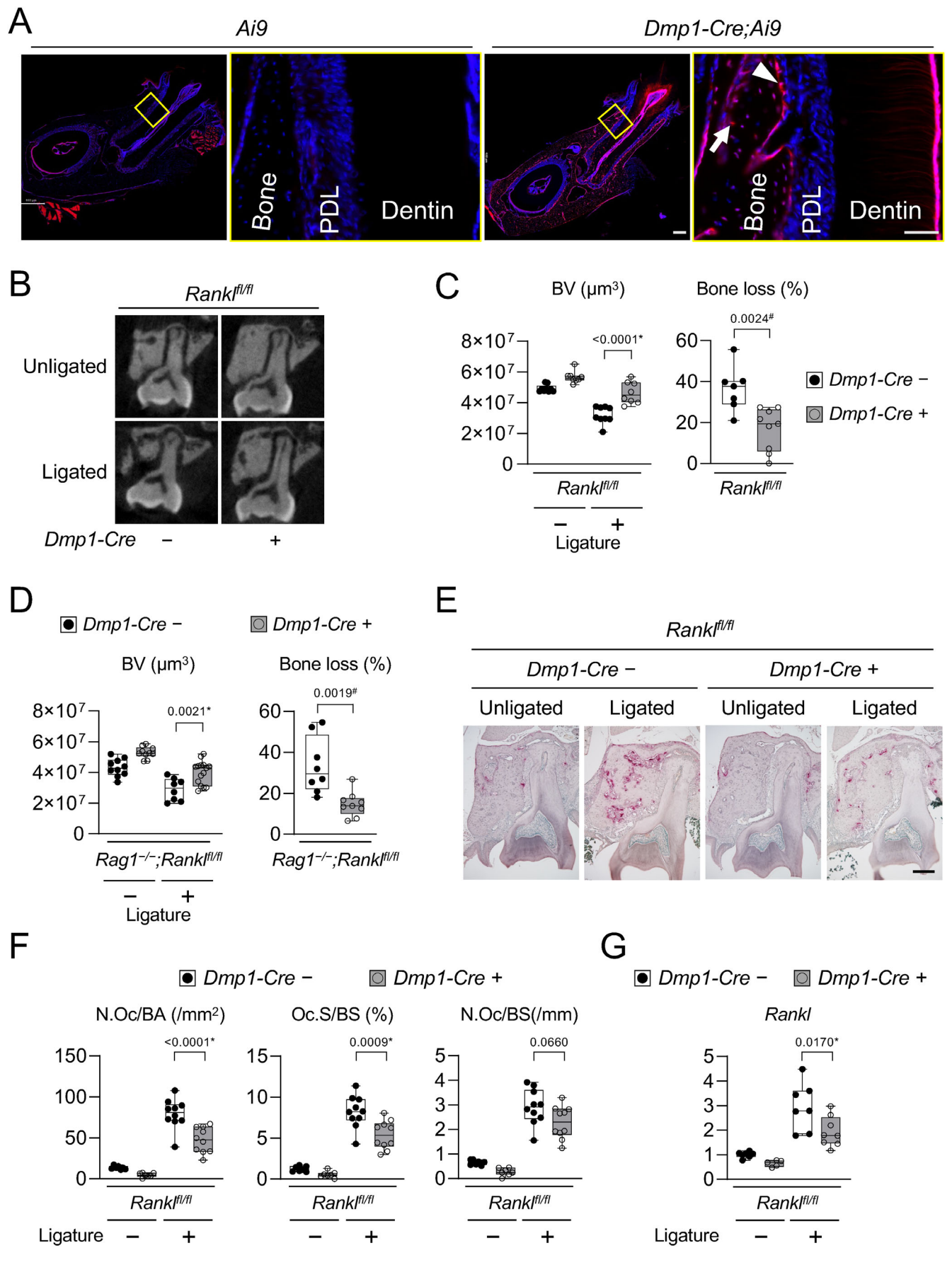


(Figure legend continues on next page.)

Unexpectedly, ligature placement dislocated the tooth before the induction of osteoclastogenesis, thereby shifting the position of the CEJ, which serves as the reference point for measuring alveolar bone height. This CEJ shift may unnaturally affect the CEJ-ABC distance, especially in the early stages of LIP. There is no doubt that measuring the CEJ-ABC distance is a reliable approach to assessing periodontal bone loss. However, it may be essential to analyze both alveolar BV and CEJ-ABC distance to identify bone loss in the LIP model accurately and sensitively. Because bone formation is not considered a typical consequence of human periodontitis, one of the major limitations of the mouse LIP model would be the significant bone formation that occurs after osteoclastic bone resorption. To reflect the pathology of bone loss found in human periodontitis, we propose to analyze alveolar bone before bone formation occurs in the LIP model. Consequently, careful pilot studies will be required to determine the appropriate time points for bone loss analysis. We have identified other previously unknown LIP phenotypes that may affect data interpretation: (i) edematous changes of PDL tissue, (ii) bacterial invasion into the lacunar of osteocytes, (iii) osteoclast induction in the absence of T/B lymphocytes. We propose that these findings are important for understanding how LIP regulates alveolar bone mass.

For decades, bacterial invasion into periodontal tissues has been known to play a key role in the etiology of human periodontitis.[65-67] We have shown that increased bacterial burden in gingival tissues coincides with gingival inflammation in LIP mice, indicating that the bacterial invasion triggers host immune responses in LIP. In human periodontitis, T and B lymphocytes are often infiltrated into gingival tissues in response to such bacterial invasion. Therefore, the role of T/B lymphocytes in alveolar bone destruction has been a major research focus in periodontology, and these lymphocytes are considered to be the primary suppliers of RANKL in periodontitis.[11,12,44-46,68,69] However, we recently used RAG1-deficient mice and demonstrated that T/B cells are not necessarily required for bone loss in *Pg*-induced periodontitis,[28] which is consistent with previous studies using different immunodeficient animal models.[70-72] We investigated the role of T/B cells in LIP-induced periodontitis and found that RAG1-deficient mice challenged with LIP exhibited bone loss comparable to wild-type mice, suggesting that T/B cells may not be critical sources of RANKL in the mouse LIP model.

Previously, Tsukasaki and colleagues showed that RANKL derived from osteoblasts and periodontal ligament cells, but not from T cells, plays a dominant role in bone loss in the LIP model.[12] In their study, however, LIP was not induced in the mice lacking RANKL predominantly in osteocytes (*Dmp1-Cre*;*Rankl*$^{fl/fl}$ mice), despite the fact that osteocyte RANKL is critical for bone resorption in a variety of conditions.[20-28] To fill this critical knowledge gap, we challenged *Dmp1-Cre*;*Rankl*$^{fl/fl}$ mice with LIP and found that these mice were protected against bone loss. Additionally, Ocy was found to have a higher capacity to express *Rankl* than Ob when stimulated with a NOD1 agonist, which was consistent with our recent findings using TLR agonists for Ocy and Ob stimulation.[28] Considering other facts that (i) *Dmp1-Cre* does not target periodontal ligament cells (the current study) or immune tissues,[28] (ii) *Dmp1-Cre* predominantly depletes RANKL in osteocytes compared with osteoblasts,[28] and (iii) osteocytes are the most abundant cells in bone,[48] our results can be interpreted to indicate that osteocytes, rather than mature osteoblasts, are the critical source of RANKL in LIP. As similar protection against bone loss was observed in *Dmp1-Cre*;*Rankl*$^{fl/fl}$ mice orally infected with periodontitis-causing bacteria, including *Pg*,[28,49] the current study will establish osteocytes as key regulators of osteoclastogenesis in periodontitis via RANKL. Importantly, *Dmp1-Cre* also targets mature osteoblasts.[73,74] Therefore, it is highly likely that osteoblast RANKL also plays an important role in bone resorption in LIP.

NOD1 and NOD2 are members of the cytosolic PRRs that are activated by peptidoglycans from Gram-positive and Gram-negative bacteria. Bacterial recognition by NOD1/2 is critical for the innate immune system to induce proinflammatory and antimicrobial responses.[75,76] In humans and mice, NOD1/2 signaling pathways are known to regulate periodontitis and periodontitis-related bone loss.[30,77-84] Specifically, in mouse LIP, activation of the NOD1 pathway, but not NOD2, has been shown to be responsible for alveolar bone resorption.[30] In contrast, the roles of TLR2 and TLR4, cell membrane receptors that recognize bacterial lipopeptides and LPS, respectively,[85] in LIP remain elusive. To determine the impact of TLR2 and TLR4 signaling pathways on bone loss in our LIP model, we challenged TLR2/4 double knockout mice with LIP. In support of a previous report,[86] we found that TLR2/4 activation is not primarily involved in the mechanism of bone loss in LIP. To reinforce this finding, we induced LIP in MYD88 knockout mice and found that even the MYD88 signaling pathway is not necessary for bone loss in LIP, suggesting that none of the activation of TLRs (except TLR3), IL-1 receptors, or IL-18 receptor is essential for driving alveolar bone loss in the LIP model.[57,87] These results contrast sharply with those in the *Pg*-induced periodontitis model, where the TLR2-MYD88 pathway is critically involved in the mechanism of bone loss.[28,88,89] Taken together, our current study and previous studies by others suggest that activation of NOD1/2 signaling may be more critical in regulating osteoclastogenesis in the LIP model. We have recently discovered that osteocytes are directly stimulated by TLR agonists and *Pg*-derived PAMPs to

*(Figure legend continued from previous page.)*

**Fig. 6.** Osteoclast induction and alveolar bone loss via osteocyte RANKL in the ligature-induced periodontitis (LIP) model. (*A*) Fluorescent microscopic images of the mandible from *Ai9* and *Dmp1-Cre;Ai9* mice. Sections were cut in the coronal plane at the medial root of the first molar. PDL = periodontal ligament tissue. An arrow indicates an osteocyte. An arrowhead indicates an osteoblast. Scale bar = 200 μm. (*B*) Two-dimensional μCT images at the middle of the second molar in the coronal plane. Five days after LIP treatment. (*C*) μCT analysis of the alveolar bone volume and percentage of alveolar bone volume loss induced by LIP. (*D*) μCT analysis of the alveolar bone volume and percentage alveolar bone volume loss induced by LIP. (*E*) TRAP staining of the jawbone tissues underneath the second molar with and without ligatures. Three days after LIP treatment. Coronal plane images. Scale bar = 200 μm. (*F*) Histomorphometry for osteoclasts on the alveolar bone underneath the ligated and unligated second molar. Three days after LIP treatment. (*G*) qPCR analysis of *Rankl* in the jawbone tissues at day 1 after LIP induction. *Hprt* was used for normalization. (*A*–*G*) Data from male mice. $^{\#}p < 0.05$ by Student's *t*-test. $^{*}p < 0.05$ by one-way ANOVA with Tukey–Kramer test.

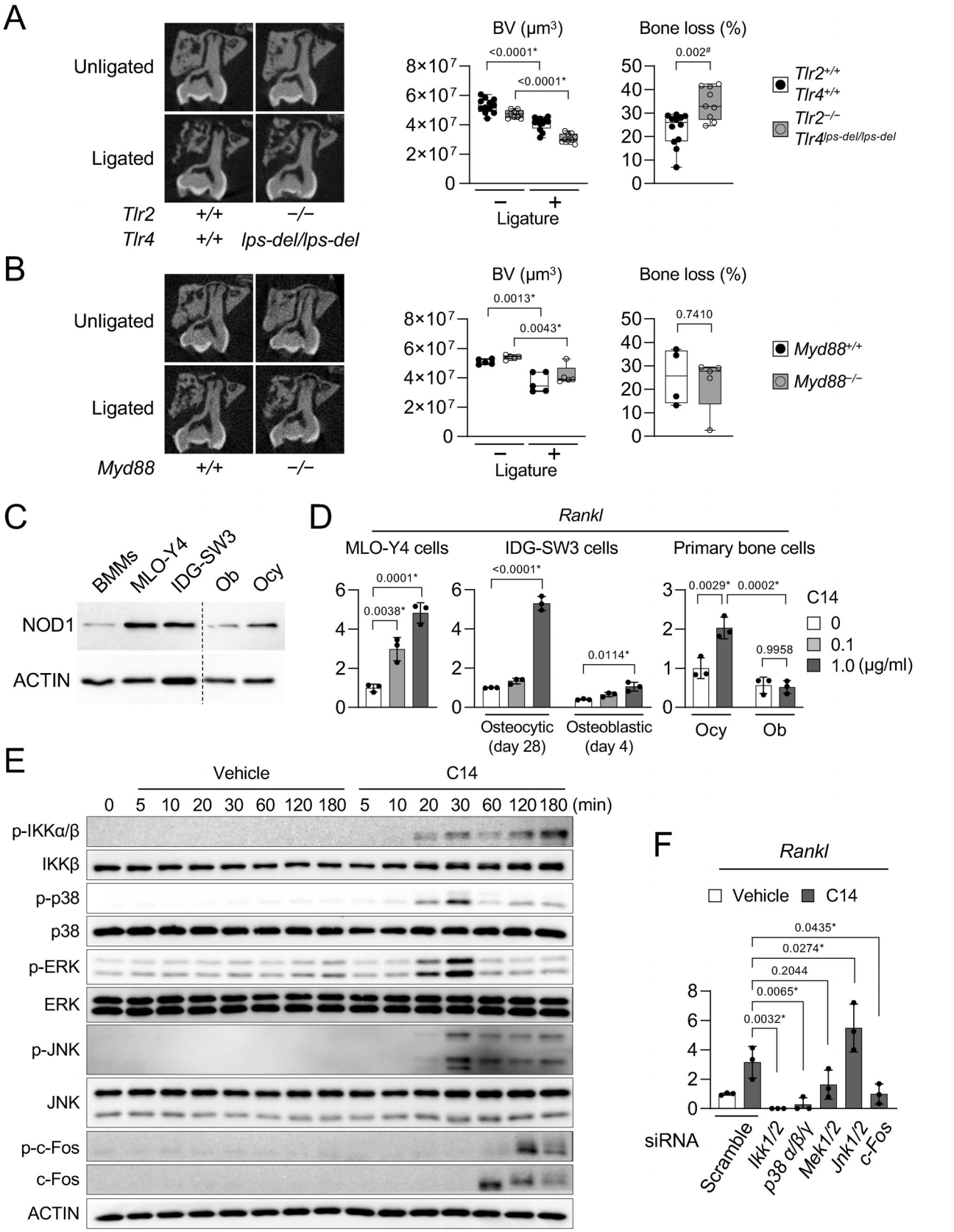


*(Figure legend continues on next page.)*

upregulate RANKL.[28] Therefore, we investigated the possibility that NOD1 signaling also directly regulates *Rankl* expression in osteocytes. Strikingly, all osteocytic cells tested were found to increase *Rankl* expression when the NOD1 pathway was activated, suggesting that the NOD1 pathway in osteocytes may directly regulate osteoclastogenesis in LIP. Downstream of NOD1, the NF-kB and p38/c-Fos signaling axes were involved in the mechanism of *Rankl* induction. Since TLR2/4 activation utilizes the ERK-CREB/STAT3 axes to induce *Rankl* expression in osteocytes,[28] it would be of interest to determine the molecular mechanisms of how activation of the NOD1 pathway promotes *Rankl* transcription via the NF-kB and p38 pathways compared with the TLR2/4-ERK-CREB/STAT3 pathway. Other osteocyte signaling pathways activated by pro-inflammatory cytokines may modulate NOD1 and its downstream signaling activation to influence the progression of bone resorption during LIP. Therefore, a direct impact of bacterially stimulated osteocytes on bone loss via RANKL can be considered in understanding the pathology of LIP and human periodontitis. Generation and analysis of osteocyte-selective NOD1- and/or NOD2-deficient mice challenged with LIP will be necessary to test this hypothesis. Further intensive genetic studies will be required to determine whether TLRs and NODs signaling pathways in osteocytes synergistically regulate LIP-induced bone resorption via RANKL. Other PAMP receptors, such as C-type lectins, may also be involved in the mechanism of LIP-induced bone loss. In human periodontitis, it might be possible that Saccharibacteria (TM7) modulates such osteocyte response to oral bacteria.[13]

In summary, we have identified previously unrecognized phenotypes of LIP, such as (i) active and dynamic bone formation after rapid and dramatic bone resorption, (ii) bacterial invasion even into the osteocyte lacunar system beyond gingival tissues, and (iii) tooth displacement that affects the outcome of CEJ-ABC measurement. Fusion of tooth roots may be another important consideration in the mouse LIP analysis, as it affects the normalization of bone volume loss. Pathologically, the lack of RANKL in osteocytes protected against bone loss in LIP, whereas RAG1 knockout mice failed to prevent it, suggesting that osteocytes are a source of RANKL in LIP. In addition, neither TLR2/4 nor MYD88 knockout mice were protected against bone loss, indicating that bacterial activation of the TLR-MYD88 pathway is not critical for osteoclastogenesis in LIP. Instead, osteocyte activation via NOD1 increased RANKL expression. These findings provide an important basis for interpreting the phenotypes of mice challenged with LIP and suggest a direct role for NOD1-activated osteocytes in the bone resorption associated with periodontitis. The NOD1-RANKL axis in osteocytes may be a therapeutic target for bone loss in periodontitis. It would be interesting to investigate whether NOD1 activation of osteocytes induces the membrane-bound or soluble form of RANKL or both in vivo. We also acknowledge the "limitations" of the current study. Because LIP may be largely influenced by the composition of oral commensal microorganisms and how oral dysbiosis develops and is established,[90] the results described in the current study may vary between animal facilities. Therefore, each laboratory needs to find the appropriate time points, parameters, and gene knockout mice when assessing the pathogenesis of LIP. Needless to say, our study does not exclude the possibility that T-cell subsets, mature osteoblasts, periodontal ligament cells, gingival fibroblasts, and MALPs regulate bone loss caused by LIP in the context of immune responses under oral microbial conditions different from those in the current study.[11,12,91,92]

## Author Contributions

**Mizuho Kittaka:** Conceptualization; writing – original draft; writing – review and editing; investigation; formal analysis; validation. **Tetsuya Yoshimoto:** Investigation; formal analysis; writing – review and editing. **Marcus E Levitan:** Investigation; formal analysis; writing – review and editing. **Rina Urata:** Investigation; formal analysis; writing – review and editing. **Roy B Choi:** Methodology; writing – review and editing. **Yayoi Teno:** Investigation; formal analysis; writing – review and editing. **Yixia Xie:** Investigation; formal analysis; writing – review and editing. **Yukiko Kitase:** Methodology; writing – review and editing. **Matthew Prideaux:** Methodology; writing – review and editing. **Sarah L Dallas:** Methodology; funding acquisition; writing – review and editing; formal analysis. **Alexander G Robling:** Methodology; writing – review and editing; resources. **Yasuyoshi Ueki:** Conceptualization; writing – original draft; writing – review and editing; funding acquisition; supervision; formal analysis; validation; investigation.

## Acknowledgments

The research reported in this publication was supported by the National Institute of Dental and Craniofacial Research (R01DE025870, R01DE025870-06S1, R21DE030561 to YU) and

*(Figure legend continued from previous page.)*

**Fig. 7.** No requirement of the TLR-MYD88 axis for bone loss in ligature-induced periodontitis (LIP) and NOD1-mediated *Rankl* induction in osteocytes. (*A*) Left: Two-dimensional μCT images at the middle of the second molar in the coronal plane. Right: μCT analysis of the alveolar bone volume and percentage of alveolar bone volume loss induced by LIP. *Tlr2*$^{-/-}$;*Tlr4*$^{lps\text{-}del/lps\text{-}del}$ and control mice were challenged with LIP for 5 days. (*B*) Left: Two-dimensional μCT images at the middle of the second molar in the coronal plane. Right: μCT analysis of the alveolar bone volume and percentage of alveolar bone volume loss induced by LIP. *Myd88*$^{-/-}$ and control mice were challenged with LIP for 5 days. (*C*) Immunoblotting for NOD1. BMMs = bone marrow-derived M-CSF-dependent macrophages. Ob = osteoblast-enriched cells from mouse calvaria; Ocy = osteocyte-enriched cells from mouse calvaria. (*D*) qPCR analysis of *Rankl* normalized by *Gapdh*. MLO-Y4 cells were stimulated with C14-Tri-LAN-Gly for 3 hours. Osteocytic (day 28) and osteoblastic (day 4) IDG-SW3 cells and primary Ocy and Ob cells were stimulated with C14-Tri-LAN-Gly for 6 hours. Representative data from three independent experiments with similar results. (*E*) Immunoblotting for signaling molecules downstream of NOD1. Cells were stimulated with C14-Tri-LAN-Gly (1 μg/mL) or vehicle for indicated times. (*F*) qPCR analysis of *Rankl* normalized by *Gapdh*. MLO-Y4 cells were transfected with siRNA for 72 hours, then stimulated with C14-Tri-LAN-Gly for 3 hours. Representative data from two independent experiments with similar results. (*A, B*) Data from male mice. (*C, E*) Immunoblotting images with molecular weight markers are presented in Supplemental Fig. S14. (*D–F*) C14 = C14-Tri-LAN-Gly. $^{\#}p < 0.05$ by Student's *t*-test. $^{*}p < 0.05$ by one-way ANOVA with Tukey–Kramer test.

by the National Institute on Aging (P01AG039355, PI project 3, SD). The content is solely the responsibility of the authors and does not necessarily represent the official views of the NIH. MK, TY, and YU thank Tianli Zhu at the Indiana University School of Dentistry Histology Core for assistance with tissue sample preparation and Caroline Miller, assistant director and laboratory manager of the Indiana University School of Medicine EM core, for EM analysis. MK is a recipient of a fellowship from the Brain Circulation Program to Develop New Leaders for International Dental Education Course through international collaborative dental research, Japan, and of a fund for young researchers from Japanese Society of Periodontology. TY is a recipient of the Japan Society for the Promotion of Science (JSPS) Overseas Research Fellowship.

## Disclosures

All authors state that they have no conflicts of interest.

## Peer Review

The peer review history for this article is available at https://www.webofscience.com/api/gateway/wos/peer-review/10.1002/jbmr.4897.

## Data Availability Statement

The data that support the findings of this study are available from the corresponding author upon reasonable request.

## References

1. Eke PI, Dye BA, Wei L, et al. Update on prevalence of periodontitis in adults in the United States: NHANES 2009 to 2012. J Periodontol. 2015;86(5):611–622.
2. Phipps KR, Stevens VJ. Relative contribution of caries and periodontal disease in adult tooth loss for an HMO dental population. J Public Health Dent. 1995;55(4):250–252.
3. Graves DT, Fine D, Teng YT, Van Dyke TE, Hajishengallis G. The use of rodent models to investigate host-bacteria interactions related to periodontal diseases. J Clin Periodontol. 2008;35(2):89–105.
4. Graves DT, Kang J, Andriankaja O, Wada K, Rossa C Jr. Animal models to study host-bacteria interactions involved in periodontitis. Front Oral Biol. 2012;15:117–132.
5. Lin P, Niimi H, Ohsugi Y, et al. Application of ligature-induced periodontitis in mice to explore the molecular mechanism of periodontal disease. Int J Mol Sci. 2021;22(16):8900.
6. Rovin S, Costich ER, Gordon HA. The influence of bacteria and irritation in the initiation of periodontal disease in germfree and conventional rats. J Periodontal Res. 1966;1(3):193–204.
7. Abe T, Hajishengallis G. Optimization of the ligature-induced periodontitis model in mice. J Immunol Methods. 2013;394(1–2):49–54.
8. Lindhe J, Ericsson I. Effect of ligature placement and dental plaque on periodontal tissue breakdown in the dog. J Periodontol. 1978;49(7):343–350.
9. Kittaka M, Yoshimoto T, Schlosser C, et al. Alveolar bone protection by targeting the SH3BP2-SYK axis in osteoclasts. J Bone Miner Res. 2020;35(2):382–395.
10. Kittaka M, Yoshimoto T, Schlosser C, et al. Microbe-dependent exacerbated alveolar bone destruction in heterozygous cherubism mice. JBMR Plus. 2020;4(6):e10352.
11. Dutzan N, Kajikawa T, Abusleme L, et al. A dysbiotic microbiome triggers TH17 cells to mediate oral mucosal immunopathology in mice and humans. Sci Transl Med. 2018;10:eaat0797.
12. Tsukasaki M, Komatsu N, Nagashima K, et al. Host defense against oral microbiota by bone-damaging T cells. Nat Commun. 2018;9(1):701.
13. Chipashvili O, Utter DR, Bedree JK, et al. Episymbiotic Saccharibacteria suppresses gingival inflammation and bone loss in mice through host bacterial modulation. Cell Host Microbe. 2021;29(11):1649–1662.e7.
14. Marchesan J, Girnary MS, Jing L, et al. An experimental murine model to study periodontitis. Nat Protoc. 2018;13(10):2247–2267.
15. Wilensky A, Gabet Y, Yumoto H, Houri-Haddad Y, Shapira L. Three-dimensional quantification of alveolar bone loss in Porphyromonas gingivalis-infected mice using micro-computed tomography. J Periodontol. 2005;76(8):1282–1286.
16. Park CH, Abramson ZR, Taba M Jr, et al. Three-dimensional micro-computed tomographic imaging of alveolar bone in experimental bone loss or repair. J Periodontol. 2007;78(2):273–281.
17. Eskan MA, Jotwani R, Abe T, et al. The leukocyte integrin antagonist Del-1 inhibits IL-17-mediated inflammatory bone loss. Nat Immunol. 2012;13(5):465–473.
18. Okamoto K, Nakashima T, Shinohara M, et al. Osteoimmunology: the conceptual framework unifying the immune and skeletal systems. Physiol Rev. 2017;97(4):1295–1349.
19. Ono T, Hayashi M, Sasaki F, Nakashima T. RANKL biology: bone metabolism, the immune system, and beyond. Inflammation Regener. 2020;40:2.
20. Xiong J, Onal M, Jilka RL, Weinstein RS, Manolagas SC, O'Brien CA. Matrix-embedded cells control osteoclast formation. Nat Med. 2011;17(10):1235–1241.
21. Shoji-Matsunaga A, Ono T, Hayashi M, Takayanagi H, Moriyama K, Nakashima T. Osteocyte regulation of orthodontic force-mediated tooth movement via RANKL expression. Sci Rep. 2017;7(1):8753.
22. Fujiwara Y, Piemontese M, Liu Y, Thostenson JD, Xiong J, O'Brien CA. RANKL (receptor activator of NFkappaB ligand) produced by osteocytes is required for the increase in B cells and bone loss caused by estrogen deficiency in mice. J Biol Chem. 2016;291(48):24838–24850.
23. Nakashima T, Hayashi M, Fukunaga T, et al. Evidence for osteocyte regulation of bone homeostasis through RANKL expression. Nat Med. 2011;17(10):1231–1234.
24. Xiong J, Piemontese M, Onal M, et al. Osteocytes, not osteoblasts or lining cells, are the main source of the RANKL required for osteoclast formation in remodeling bone. PloS One. 2015;10(9):e0138189.
25. Piemontese M, Xiong J, Fujiwara Y, Thostenson JD, O'Brien CA. Cortical bone loss caused by glucocorticoid excess requires RANKL production by osteocytes and is associated with reduced OPG expression in mice. Am J Physiol Endocrinol Metab. 2016;311(3):E587–E593.
26. Xiong J, Piemontese M, Thostenson JD, Weinstein RS, Manolagas SC, O'Brien CA. Osteocyte-derived RANKL is a critical mediator of the increased bone resorption caused by dietary calcium deficiency. Bone. 2014;66:146–154.
27. Kim HN, Xiong J, MacLeod RS, et al. Osteocyte RANKL is required for cortical bone loss with age and is induced by senescence. JCI Insight. 2020;5(19):e138815.
28. Yoshimoto T, Kittaka M, Doan AAP, et al. Osteocytes directly regulate osteolysis via MYD88 signaling in bacterial bone infection. Nat Commun. 2022;13(1):6648.
29. Yu K, Ma Y, Li X, et al. Lipopolysaccharide increases IL-6 secretion via activation of the ERK1/2 signaling pathway to up-regulate RANKL gene expression in MLO-Y4 cells. Cell Biol Int. 2017;41(1):84–92.
30. Jiao Y, Darzi Y, Tawaratsumida K, et al. Induction of bone loss by pathobiont-mediated Nod1 signaling in the oral cavity. Cell Host Microbe. 2013;13(5):595–601.
31. Kim JE, Nakashima K, de Crombrugghe B. Transgenic mice expressing a ligand-inducible cre recombinase in osteoblasts and odontoblasts: a new tool to examine physiology and disease of postnatal bone and tooth. Am J Pathol. 2004;165(6):1875–1882.
32. Schneider CA, Rasband WS, Eliceiri KW. NIH image to ImageJ: 25 years of image analysis. Nat Methods. 2012;9(7):671–675.

33. Maurel DB, Matsumoto T, Vallejo JA, et al. Characterization of a novel murine Sost ER(T2) Cre model targeting osteocytes. Bone Res. 2019; 7:6.
34. Wang Q, Garrity GM, Tiedje JM, Cole JR. Naive Bayesian classifier for rapid assignment of rRNA sequences into the new bacterial taxonomy. Appl Environ Microbiol. 2007;73(16):5261–5267.
35. Bolyen E, Rideout JR, Dillon MR, et al. Reproducible, interactive, scalable and extensible microbiome data science using QIIME 2. Nat Biotechnol. 2019;37(8):852–857.
36. Kato Y, Windle JJ, Koop BA, Mundy GR, Bonewald LF. Establishment of an osteocyte-like cell line, MLO-Y4. J Bone Miner Res. 1997; 12(12):2014–2023.
37. Woo SM, Rosser J, Dusevich V, Kalajzic I, Bonewald LF. Cell line IDG-SW3 replicates osteoblast-to-late-osteocyte differentiation in vitro and accelerates bone formation in vivo. J Bone Miner Res. 2011; 26(11):2634–2646.
38. Erben RG. Bone-labeling techniques. In An YH, Martin KL, eds. Handbook of histology methods for bone and cartilage. Totowa, NJ: Humana Press; 2003 pp 99–117.
39. Stashenko P, Fujiyoshi P, Obernesser MS, Prostak L, Haffajee AD, Socransky SS. Levels of interleukin 1 beta in tissue from sites of active periodontal disease. J Clin Periodontol. 1991;18(7):548–554.
40. Stashenko P, Jandinski JJ, Fujiyoshi P, Rynar J, Socransky SS. Tissue levels of bone resorptive cytokines in periodontal disease. J Periodontol. 1991;62(8):504–509.
41. Cardoso CR, Garlet GP, Crippa GE, et al. Evidence of the presence of T helper type 17 cells in chronic lesions of human periodontal disease. Oral Microbiol Immunol. 2009;24(1):1–6.
42. Fujihashi K, Yamamoto M, Hiroi T, Bamberg TV, McGhee JR, Kiyono H. Selected Th1 and Th2 cytokine mRNA expression by CD4(+) T cells isolated from inflamed human gingival tissues. Clin Exp Immunol. 1996;103(3):422–428.
43. Johnson RB, Wood N, Serio FG. Interleukin-11 and IL-17 and the pathogenesis of periodontal disease. J Periodontol. 2004;75(1):37–43.
44. Seymour GJ, Crouch MS, Powell RN, et al. The identification of lymphoid cell subpopulations in sections of human lymphoid tissue and gingivitis in children using monoclonal antibodies. J Periodontal Res. 1982;17(3):247–256.
45. Seymour GJ, Gemmell E, Walsh LJ, Powell RN. Immunohistological analysis of experimental gingivitis in humans. Clin Exp Immunol. 1988;71(1):132–137.
46. Kawai T, Matsuyama T, Hosokawa Y, et al. B and T lymphocytes are the primary sources of RANKL in the bone resorptive lesion of periodontal disease. Am J Pathol. 2006;169(3):987–998.
47. Mombaerts P, Iacomini J, Johnson RS, Herrup K, Tonegawa S, Papaioannou VE. RAG-1-deficient mice have no mature B and T lymphocytes. Cell. 1992;68(5):869–877.
48. Robling AG, Bonewald LF. The osteocyte: new insights. Annu Rev Physiol. 2020;82:485–506.
49. Graves DT, Alshabab A, Albiero ML, et al. Osteocytes play an important role in experimental periodontitis in healthy and diabetic mice through expression of RANKL. J Clin Periodontol. 2018;45(3): 285–292.
50. Zhong ZA, Sun W, Chen H, et al. Optimizing tamoxifen-inducible Cre/loxp system to reduce tamoxifen effect on bone turnover in long bones of young mice. Bone. 2015;81:614–619.
51. Hofbauer LC, Lacey DL, Dunstan CR, Spelsberg TC, Riggs BL, Khosla S. Interleukin-1beta and tumor necrosis factor-alpha, but not interleukin-6, stimulate osteoprotegerin ligand gene expression in human osteoblastic cells. Bone. 1999;25(3):255–259.
52. Mori T, Miyamoto T, Yoshida H, et al. IL-1beta and TNFalpha-initiated IL-6-STAT3 pathway is critical in mediating inflammatory cytokines and RANKL expression in inflammatory arthritis. Int Immunol. 2011; 23(11):701–712.
53. Wu Q, Zhou X, Huang D, Ji Y, Kang F. IL-6 enhances osteocyte-mediated osteoclastogenesis by promoting JAK2 and RANKL activity in vitro. Cell Physiol Biochem. 2017;41(4):1360–1369.
54. Kotake S, Udagawa N, Takahashi N, et al. IL-17 in synovial fluids from patients with rheumatoid arthritis is a potent stimulator of osteoclastogenesis. J Clin Invest. 1999;103(9):1345–1352.
55. Li JY, Yu M, Tyagi AM, et al. IL-17 receptor signaling in osteoblasts/osteocytes mediates PTH-induced bone loss and enhances osteocytic RANKL production. J Bone Miner Res. 2019; 34(2):349–360.
56. Sakamoto E, Kido J-i, Takagi R, et al. Advanced glycation end-product 2 and Porphyromonas gingivalis lipopolysaccharide increase sclerostin expression in mouse osteocyte-like cells. Bone. 2019;122:22–30.
57. O'Neill LA, Bowie AG. The family of five: TIR-domain-containing adaptors in toll-like receptor signalling. Nat Rev Immunol. 2007;7(5): 353–364.
58. Onal M, St John HC, Danielson AL, Pike JW. Deletion of the distal Tnfsf11 RL-D2 enhancer that contributes to PTH-mediated RANKL expression in osteoblast lineage cells results in a high bone mass phenotype in mice. J Bone Miner Res. 2016;31(2):416–429.
59. Parrish LC, Kretzschmar DP, Swan RH. Osteomyelitis associated with chronic periodontitis: a report of three cases. J Periodontol. 1989; 60(12):716–722.
60. Van den Bossche LH, Demeulemeester JDA, Bossuyt MH. Periodontal infection leading to periostitis ossificans (''Garre's osteomyelitis'') of the mandible. Report of a case. J Periodontol. 1993;64(1):60–62.
61. de Mesy Bentley KL, Trombetta R, Nishitani K, et al. Evidence of staphylococcus aureus deformation, proliferation, and migration in canaliculi of live cortical bone in murine models of osteomyelitis. J Bone Miner Res. 2017;32(5):985–990.
62. Yang DQ, Wijenayaka AR, Solomon LB, et al. Novel insights into Staphylococcus aureus deep bone infections: the involvement of osteocytes. mBio. 2018;9(2):e00145–e00148.
63. de Mesy Bentley KL, MacDonald A, Schwarz EM, Oh I. Chronic osteomyelitis with Staphylococcus aureus deformation in submicron canaliculi of osteocytes: a case report. JBJS Case Connect. 2018;8(1):e8.
64. Al-Sosowa AA, Alhajj MN, Abdulghani EA, et al. Three-dimensional analysis of alveolar bone with and without periodontitis. Int Dent J. 2022;72(5):634–640.
65. Gillett R, Johnson NW. Bacterial invasion of the periodontium in a case of juvenile periodontitis. J Clin Periodontol. 1982;9(1):93–100.
66. Allenspach-Petrzilka GE, Guggenheim B. Bacterial invasion of the periodontium; an important factor in the pathogenesis of periodontitis? J Clin Periodontol. 1983;10(6):609–617.
67. Ji S, Choi YS, Choi Y. Bacterial invasion and persistence: critical events in the pathogenesis of periodontitis? J Periodontal Res. 2015;50(5): 570–585.
68. Hajishengallis G, Chavakis T, Lambris JD. Current understanding of periodontal disease pathogenesis and targets for host-modulation therapy. Periodontol 2000. 2000;84(1):14–34.
69. Ikeuchi T, Moutsopoulos NM. Osteoimmunology in periodontitis; a paradigm for Th17/IL-17 inflammatory bone loss. Bone. 2022;163: 116500.
70. Klausen B, Hougen HP, Fiehn NE. Increased periodontal bone loss in temporarily B lymphocyte-deficient rats. J Periodontal Res. 1989; 24(6):384–390.
71. Guggenheim B, Gaegauf-Zollinger R, Hefti A, Burckhardt JJ. The effect of cyclosporin A on periodontal disease in rats monoassociated with Actinomyces viscosus Ny 1. J Periodontal Res. 1981;16(1):26–38.
72. Baker PJ, Evans RT, Roopenian DC. Oral infection with Porphyromonas gingivalis and induced alveolar bone loss in immunocompetent and severe combined immunodeficient mice. Arch Oral Biol. 1994; 39(12):1035–1040.
73. Lim J, Burclaff J, He G, Mills JC, Long F. Unintended targeting of Dmp1-Cre reveals a critical role for Bmpr1a signaling in the gastrointestinal mesenchyme of adult mice. Bone Res. 2017;5:16049.
74. Zhang J, Link DC. Targeting of mesenchymal stromal cells by Cre-recombinase transgenes commonly used to target osteoblast lineage cells. J Bone Miner Res. 2016;31(11):2001–2007.
75. Caruso R, Warner N, Inohara N, Nunez G. NOD1 and NOD2: signaling, host defense, and inflammatory disease. Immunity. 2014;41(6):898–908.

76. Philpott DJ, Sorbara MT, Robertson SJ, Croitoru K, Girardin SE. NOD proteins: regulators of inflammation in health and disease. Nat Rev Immunol. 2014;14(1):9–23.
77. Prates TP, Taira TM, Holanda MC, et al. NOD2 contributes to Porphyromonas gingivalis-induced bone resorption. J Dent Res. 2014;93(11): 1155–1162.
78. Souza JA, Medeiros MC, Rocha FR, et al. Role of NOD2 and RIP2 in host-microbe interactions with Gram-negative bacteria: insights from the periodontal disease model. Innate Immun. 2016;22(8): 598–611.
79. Yuan H, Zelkha S, Burkatovskaya M, Gupte R, Leeman SE, Amar S. Pivotal role of NOD2 in inflammatory processes affecting atherosclerosis and periodontal bone loss. Proc Natl Acad Sci U S A. 2013;110(52): E5059–E5068.
80. Sudo T, Okada Y, Ozaki K, et al. Association of NOD2 mutations with aggressive periodontitis. J Dent Res. 2017;96(10):1100–1105.
81. Mizuno N, Kume K, Nagatani Y, et al. Aggressive periodontitis and NOD2 variants. J Hum Genet. 2020;65(10):841–846.
82. Folwaczny M, Glas J, Torok HP, Mauermann D, Folwaczny C. The 3020insC mutation of the NOD2/CARD15 gene in patients with periodontal disease. Eur J Oral Sci. 2004;112(4):316–319.
83. He Y, Wu Z, Chen S, et al. Activation of the pattern recognition receptor NOD1 in periodontitis impairs the osteogenic capacity of human periodontal ligament stem cells via p38/MAPK signalling. Cell Prolif. 2022;55(12):e13330.
84. Chaves de Souza JA, Frasnelli SC, Curylofo-Zotti FA, et al. NOD1 in the modulation of host-microbe interactions and inflammatory bone resorption in the periodontal disease model. Immunology. 2016; 149(4):374–385.
85. Akira S, Uematsu S, Takeuchi O. Pathogen recognition and innate immunity. Cell. 2006;124(4):783–801.
86. Lin M, Hu Y, Wang Y, Kawai T, Wang Z, Han X. Different engagement of TLR2 and TLR4 in Porphyromonas gingivalis vs. ligature-induced periodontal bone loss. Braz Oral Res. 2017;31:e63.
87. Adachi O, Kawai T, Takeda K, et al. Targeted disruption of the MyD88 gene results in loss of IL-1- and IL-18-mediated function. Immunity. 1998;9(1):143–150.
88. Burns E, Bachrach G, Shapira L, Nussbaum G. Cutting edge: TLR2 is required for the innate response to Porphyromonas gingivalis: activation leads to bacterial persistence and TLR2 deficiency attenuates induced alveolar bone resorption. J Immunol. 2006;177(12):8296–8300.
89. Papadopoulos G, Weinberg EO, Massari P, et al. Macrophage-specific TLR2 signaling mediates pathogen-induced TNF-dependent inflammatory oral bone loss. J Immunol. 2013;190(3):1148–1157.
90. Arce M, Endo N, Dutzan N, Abusleme L. A reappraisal of microbiome dysbiosis during experimental periodontitis. Mol Oral Microbiol. 2022;37(5):180–195.
91. Kondo T, Okawa H, Hokugo A, et al. Oral microbial extracellular DNA initiates periodontitis through gingival degradation by fibroblast-derived cathepsin K in mice. Commun Biol. 2022;5(1):962.
92. Yu W, Zhong L, Yao L, et al. Bone marrow adipogenic lineage precursors promote osteoclastogenesis in bone remodeling and pathologic bone loss. J Clin Invest. 2021;131(2):e140214.